AGU PUBLICATIONS

JGR

Journal of Geophysical Research: Solid Earth

RESEARCH ARTICLE

10.1002/2014JB011040

Key Points:
- The breakup magmatism at the Vøring margin is caused by high mantle temperature
- The first 2 Ma of magmatism after breakup is augmented by a secondary process
- The Vøring Spur off the margin is created by a secondary Miocene magmatic event

Supporting Information:
- Readme
- Figures S1–S19

Correspondence to:
A. Breivik,
a.j.breivik@geo.uio.no

Citation:
Breivik, A., J. I. Faleide, R. Mjelde, E. Flueh, and Y. Murai (2014), Magmatic development of the outer Vøring margin from seismic data, *J. Geophys. Res. Solid Earth*, *119*, 6733–6755, doi:10.1002/2014JB011040.

Received 11 FEB 2014
Accepted 10 JUL 2014
Accepted article online 17 JUL 2014
Published online 5 SEP 2014

Magmatic development of the outer Vøring margin from seismic data

Asbjørn Breivik[1], Jan Inge Faleide[1], Rolf Mjelde[2], Ernst Flueh[3], and Yoshio Murai[4]

[1]Department of Geosciences, University of Oslo, Oslo, Norway, [2]Department of Earth Science, University of Bergen, Bergen, Norway, [3]IFM-Geomar, Leibniz-Institute for Marine Sciences, Kiel, Germany, [4]Institute of Seismology and Volcanology, Hokkaido University, Sapporo, Japan

Abstract The Vøring Plateau off mid-Norway is a volcanic passive margin, located north of the East Jan Mayen Fracture Zone (EJMFZ). Large volumes of magmatic rocks were emplaced during Early Eocene margin formation. In 2003, an ocean bottom seismometer survey was acquired over the margin. One profile crosses from the Vøring Plateau to the Vøring Spur, a bathymetric high north of the EJMFZ. The *P* wave data were ray traced into a 2-D crustal velocity model. The velocity structure of the Vøring Spur indicates up to 15 km igneous crustal thickness. Magmatic processes can be estimated by comparing seismic velocity (V_P) with igneous thickness (H). This and two other profiles show a positive H-V_P correlation at the Vøring Plateau, consistent with elevated mantle temperature at breakup. However, during the first 2 Ma magma production was augmented by a secondary process, possibly small-scale convection. From ~51.5 Ma excess melting may be caused by elevated mantle temperature alone. Seismic stratigraphy around the Vøring Spur shows that it was created by at least two uplift events, with the main episode close to the Miocene/Pliocene boundary. Low H-V_P correlation of the spur is consistent with renewed igneous growth by constant, moderate-degree mantle melting, not related to the breakup magmatism. The admittance function between bathymetry and free-air gravity shows that the high is near local isostatic equilibrium, precluding that compressional flexure at the EJMFZ uplifted the high. We find a proposed Eocene triple junction model for the margin to be inconsistent with observations.

1. Introduction

Extensive breakup magmatism affected large parts of the Northeast Atlantic in the Paleocene/Early Eocene, constituting a large part of the Northeast Atlantic Igneous Province (NAIP) [e.g., *White et al.*, 1987; *Eldholm and Grue*, 1994]. After the breakup magmatism died down to normal seafloor spreading levels elsewhere, magmatism may have been continuous along the Faeroes-Iceland/Greenland-Iceland Ridge (FIR/GIR; Figure 1). The formation of the NAIP has been tied to the Iceland hot spot, believed to be caused by a long-lived mantle plume transporting hotter mantle material from a deep thermal boundary layer [*Forsyth et al.*, 1986; *Lawver and Müller*, 1994; *Storey et al.*, 2007]. The magmatism is not uniformly distributed along the margins, and both the magnitude and duration are variable [e.g., *Berndt et al.*, 2001]. South of the FIR/GIR, magmatism abates away from the Iceland hot spot [*Holbrook et al.*, 2001]. This is also the case north of the FIR/GIR. The breakup magmatism is strong north of the Faeroes [*Parkin et al.*, 2007; *Parkin and White*, 2008; *White et al.*, 2008] but significantly reduced at the northern Møre Margin [*Breivik et al.*, 2006]. The conjugate east Jan Mayen microcontinent volcanic margin shows the same distribution [*Breivik et al.*, 2012]. However, the breakup magmatism increases again on the Vøring margin to the north [*Mjelde et al.*, 2005; *Breivik et al.*, 2009], and on the conjugate Northeast Greenland margin [*Voss and Jokat*, 2007].

There is also renewed magmatic activity in several other areas in the Northeast Atlantic, outside of Iceland. Best known may be the Jan Mayen magmatism creating the island with the still active stratovolcano Beerenberg, sourced from low-degree mantle melting [*Trønnes et al.*, 1999] (Figure 1). The Eggvin Bank between Jan Mayen and Greenland was created by high magmatic productivity, possibly mostly on axis at the northernmost Kolbeinsey Ridge from the Late Oligocene to present [*Mertz et al.*, 2004]. North of that, the isolated intraplate Vesteris Seamount was active recently [*Haase and Devey*, 1994]. Also, the Northeast Greenland margin experienced significant magmatism around Traill Ø at the Eocene-Oligocene transition [*Noble et al.*, 1988; *Price et al.*, 1997].

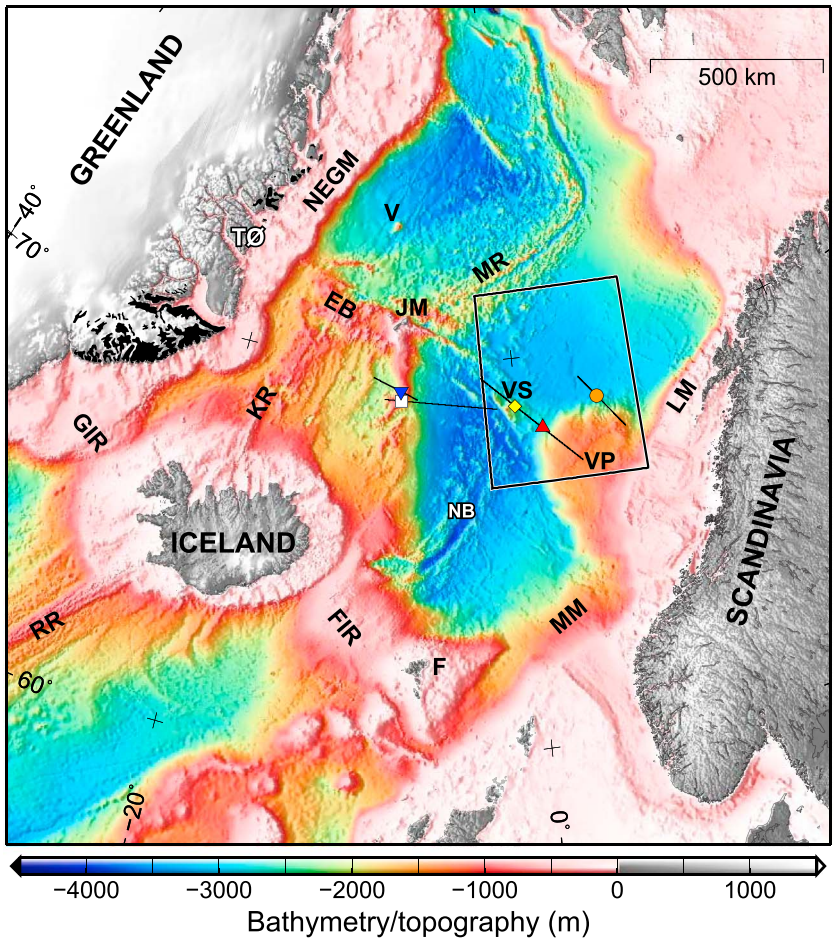

Figure 1. Regional location map based on ETOPO-2 bathymetry/topography [*Sandwell and Smith*, 1997] showing positions of various features discussed in the text. Black areas onshore Greenland indicate early Cenozoic basalt flows or intrusions. AR: Aegir Ridge, EB: Eggvin Bank, F: Faeroes, FIR: Faeroes-Iceland Ridge, GIR: Greenland-Iceland Ridge, JM: Jan Mayen, KR: Kolbeinsey Ridge, LM: Lofoten Margin, MM: Møre Margin, MR: Mohn Ridge, NB: Norway Basin, NEGM: Northeast Greenland Margin, RR: Reykjanes Ridge, TØ: Traill Ø, VP: Vøring Plateau, VS: Vøring Spur, and V: Vesteris Seamount. Positions of some of the 1-D velocity profiles derived from ocean bottom seismometer (OBS) profiles shown in Figure 12a are indicated by color symbols. The frame shows the position of Figure 2.

The seismic data were acquired as part of the 2003 Euromargins survey over the Vøring and Lofoten margins, with lines extending far into the oceanic basin in order to examine the complete development of the breakup magmatism. The shot line analyzed here is 379 km long, and we deployed 21 ocean bottom seismometers/hydrophones (OBS/H) to record seismic traveltimes (Figure 2). It targeted a bathymetric high located off the Vøring Plateau, the Vøring Spur, because its origin was not obvious. Initially, we considered it to be either a continental fragment, or more likely to be formed by the last remnant of the breakup magmatism. However, subsequent analysis of available reflection seismic data in the area pointed to a different origin altogether. Based on the deformation pattern of sediments around the high, *Breivik et al.* [2008] argued that the Vøring Spur was formed by secondary magmatic growth of the oceanic crust, uplifting the high in the Late Miocene. An alternative model by *Gernigon et al.* [2009] proposed that the high formed at a hypothesized triple junction tapping breakup magmatism during early seafloor spreading.

Breivik et al. [2008] presented the velocity model of Profile 11-03 to constrain the igneous crustal thickness under the high, used to estimate magma volume. Here we document the seismic data and the velocity modeling of the profile, not shown before. We proceed to analyze the velocity structure in order to constrain the magmatic processes behind the excess breakup magmatism and that of the formation of the Vøring Spur. We similarly analyze the adjacent Profile 1-99 [*Mjelde et al.*, 2005] and compare the results to that of *Breivik et al.* [2009] from the northern Vøring Plateau. From this we derive a development model for the breakup

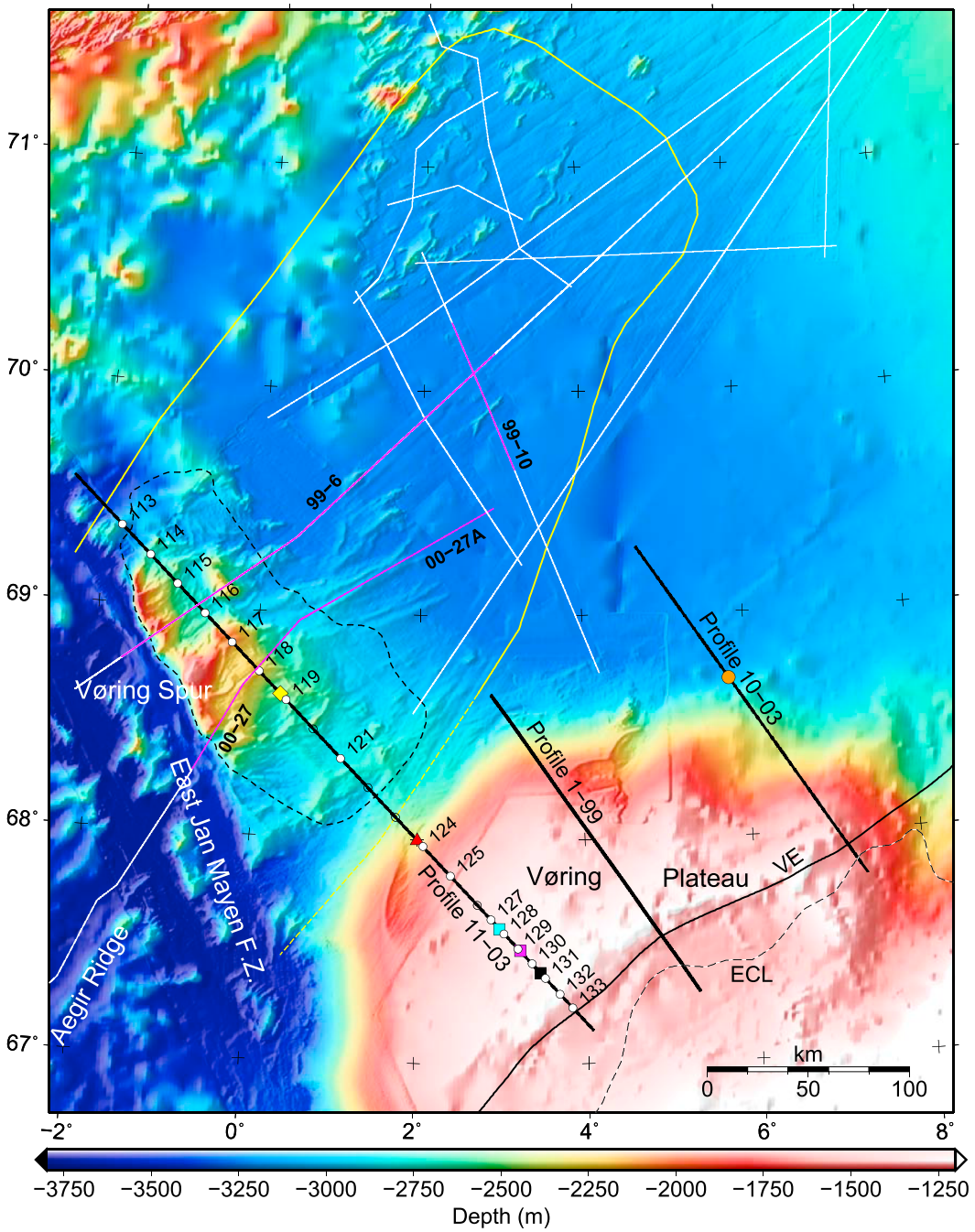

Figure 2. International Bathymetric Chart of the Arctic Ocean (IBCAO) (v.2) bathymetry [*Jakobsson et al.*, 2008] with high-resolution side scan bathymetry overlay. The location of OBS profiles discussed is shown with black lines. Instrument locations for Profile 11-03 are marked with circles; those returning useful data are white filled and annotated. Multichannel seismic (MCS) survey lines are shown in white, with seismic example locations marked in magenta. Dashed line shows extent of thick crust under the Vøring Spur, while yellow line shows the extent of the inversion event mapped from the MCS profiles [*Breivik et al.*, 2008]. Positions of additional 1-D velocity profiles shown in Figure 12 are indicated by color symbols. ECL: Eastern limit Cenozoic lavas; VE: Vøring Escarpment [*Skogseid*, 1994].

magmatism of this margin segment. Finally, we compute the admittance function between the bathymetry and free-air gravity to find the compensation mechanism of the Vøring Spur.

2. Data Acquisition and Processing

The survey was performed during the summer of 2003 by the R/V *Håkon Mosby*, in cooperation between the Department of Geosciences, Universities of Oslo, Norway; the Department of Earth Science, University

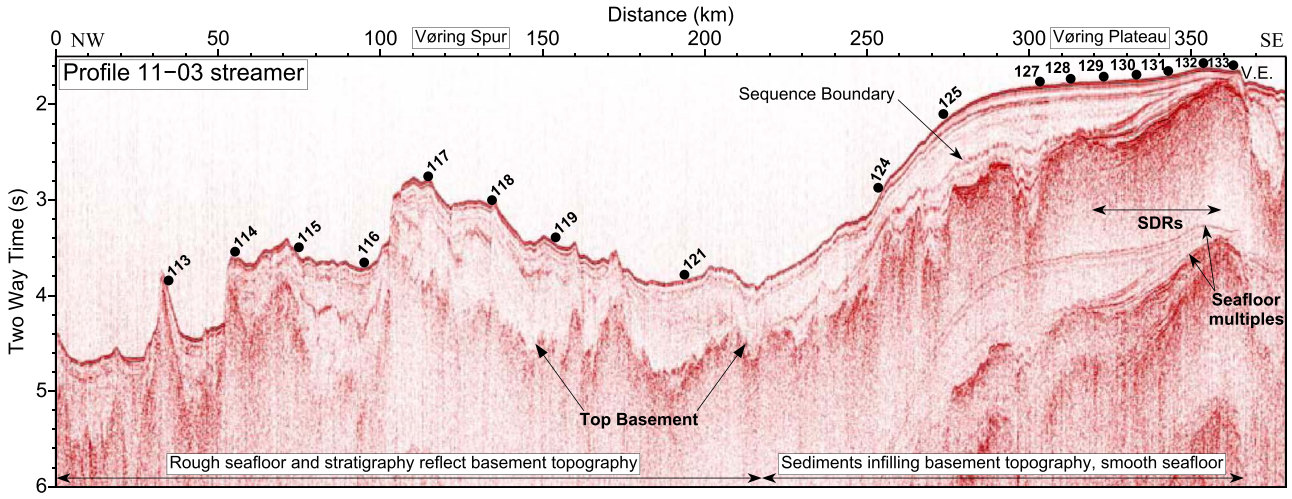

Figure 3. Single-channel streamer reflection seismic data of Profile 11-03. OBS/H locations are shown with filled black circles, with the instrument number above. SDRs: Seaward Dipping Reflectors; VE: Vøring Escarpment.

of Bergen, Norway; GEOMAR, Kiel, Germany; and the Institute for Seismology and Volcanology (ISV), Hokkaido University, Sapporo, Japan. Four air guns with a total volume of 78.66 L (4800 in^3) were fired every 200 m at a tow depth of 12 m. The data were recorded by ocean bottom seismometers (OBSs), consisting of ISV three-component analog or digital seismometers, or by GEOMAR digital three-component seismometers with additional hydrophone, or by hydrophone alone (OBH). Navigation was by the Differential Global Positioning System.

Preprocessing consisted of extracting a 60 s record length after each shot, adjusting time drift, tying to navigation, and correcting for physical instrument drift along profile due to oceanic currents as it settles to the bottom. Processing included debiasing, band-pass filtering (6–12 Hz), and automatic gain control (2 s window) or offset-dependent scaling. Initial processing was then compared to processing including spiking predictive deconvolution. All seismic examples shown here are based on the latter. The record sections are velocity reduced with 8 km s^{-1}. Vertical reflections from the shots were also recorded by a single-channel streamer (SCS, Figure 3). The streamer profile was processed with spiking deconvolution, band-pass filtering (20–60 Hz), and exponential amplitude scaling with time. The signal is minimum phase.

Magnetic data were logged every 5 s during seismic shooting by a GeoMetrics G 801 proton precession magnetometer towed 180 m behind the ship. The data were adjusted for short-term field fluctuations measured from a base station (Rørvik, Norway) and corrected to the International Geomagnetic Reference Field 10. The recording was done during a magnetic quiet period. Final smoothing was performed with a Gaussian spatial filter 10 km wide.

In addition, we show bathymetric data collected for the Norwegian Petroleum Directorate (NPD) in 2000 and 2001 by Fugro-Geoteam with a Simrad EM 120 echo sounder (Figure 2). The 100 m data grid was gridded with 0.002° longitude and 0.001° latitude grid cell size, using the Generic Mapping Tools program surface with tension set to 0.75 [*Smith and Wessel*, 1990; *Wessel and Smith*, 1998]. This was merged with the IBCAO-2 bathymetry [*Jakobsson et al.*, 2008] (identical to IBCAO-3 here) to fill in uncovered areas.

3. *P* Wave Modeling

We use ray tracing software for the velocity modeling [*Zelt and Smith*, 1992]. The Rayinvr program has node-specific inversion functionality, useful for finding solutions involving multiple receivers. The model is built layer by layer from the top on downward by fitting the traveltimes from consecutively larger offsets. We use measured bathymetry, and the sediment thickness initially estimated from the single-channel reflection seismic line (Figure 3). The sedimentary package was subdivided into two layers for the part east of 210 km in the model, where the younger sequence onlaps the older at the indicated boundary. To make the initial model, the interpretation was depth converted using 1.9 km s^{-1} for the upper and 2.1 km s^{-1} for the lower

Table 1. Seismic Model Fit Statistics for Individual Major Phases and Summary for All Phases[a]

Phase	No. Rays	RMS Δt (ms)	χ^2
Water	223	52	1.070
P_g1	247	55	0.531
P_g2	346	61	0.589
P_g3	553	68	0.600
P_g4	650	60	0.397
P_g5	810	70	0.481
P_n	265	90	0.462
P_MP	653	89	0.521
All phases	3899	71	0.537

[a]Shallower reflections do not constrain velocity significantly but are included in the total phase count.

sedimentary section, based on earlier OBS studies [e.g., *Mjelde et al.*, 2001]. A seaward dipping reflector (SDR) sequence is seen west of the Vøring escarpment, between 320 km and 360 km on the SCS profile.

To estimate the goodness of fit between the model reproduction and the observed traveltimes, the software makes use of the χ^2 analysis. This weighs the degree of fit to the uncertainty of the interpretation, where a value of 1 or lower defines a fit. The uncertainty of the interpretation is here usually set to be approximately ±1 cycle of the phase, which increases with depth and offset. This reflects that it is often difficult to pick the first onset of an arrival due to noise and artifacts. There is also uncertainty in shot timing, the instrument location, and the bathymetry [*Hooft et al.*, 2000]. For the short offset arrivals from the sedimentary layers, this has been estimated to ±50 ms, while Moho arrivals are assigned an uncertainty of ±100 ms where they stand out clearly. In some cases where the arrival is weak and difficult to pick, a greater uncertainty is assigned. The arrivals from most of the main layer boundaries of the profiles have been modeled to a fit $\chi^2 \leq 1$ (Table 1).

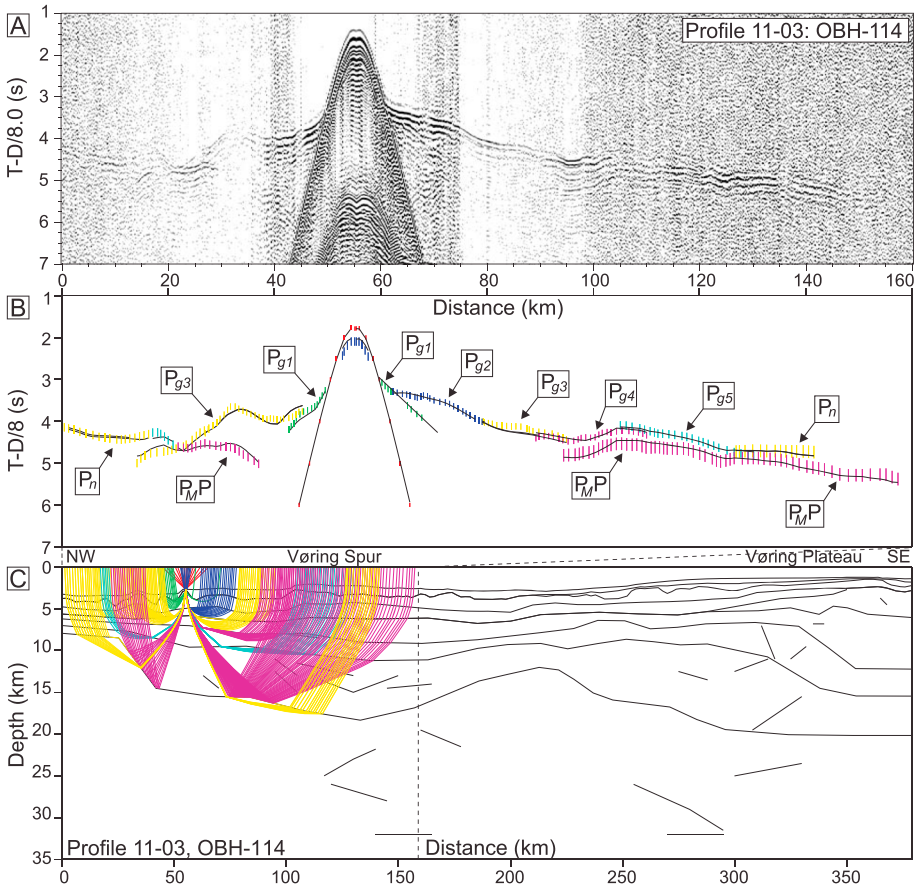

Figure 4. Data, interpretation, and ray tracing of OBH 114, Profile 11-03, Vøring Spur. (a) Hydrophone data, offset-dependent scaling. (b) Arrival time interpretation and model reproduction. Phase picks are shown by vertical bars, where the height of the bar shows interpretation uncertainty. Calculated times for each phase are shown by solid black lines. (c) Ray tracing of the velocity model. Ray colors correspond to the pick bar colors in Figure 4b.

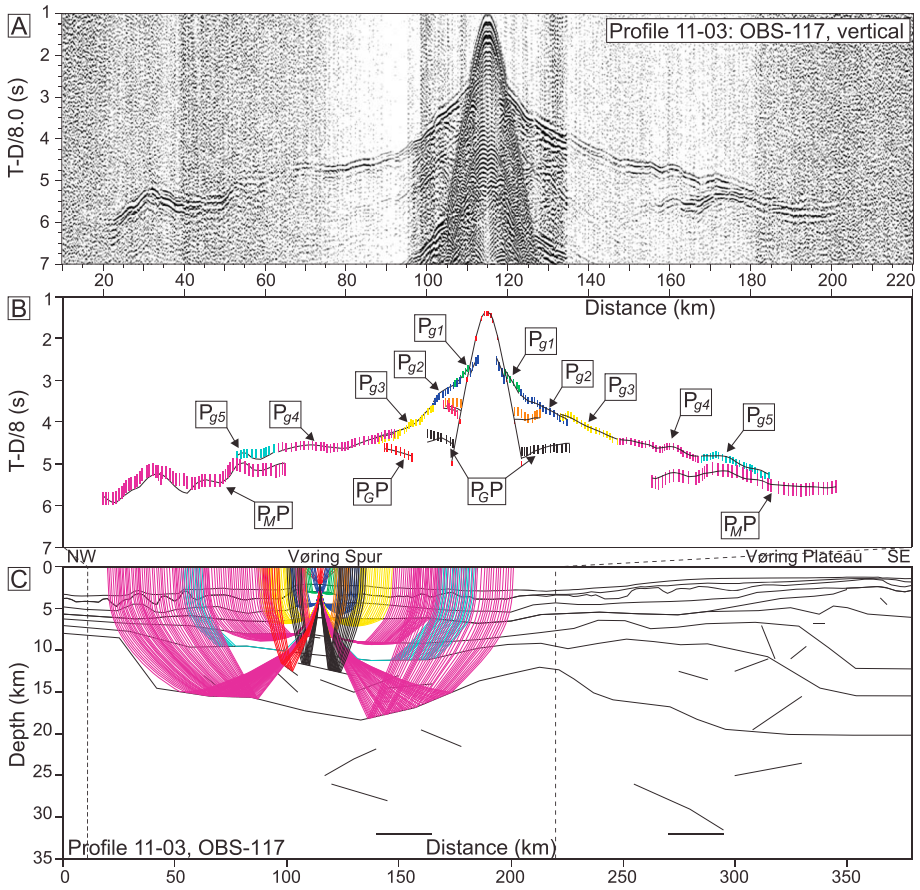

Figure 5. Data, interpretation, and ray tracing of OBS 117, Profile 11-03, Vøring Spur. (a) OBS data, vertical component, and offset-dependent scaling. (b) Arrival time interpretation and model reproduction. Phase picks are shown by vertical bars, where the height of the bar shows interpretation uncertainty. Calculated times for each phase are shown by solid black lines. (c) Ray tracing of the velocity model. Ray colors correspond to the pick bar colors in Figure 5b.

Of the 21 OBSs deployed, OBSs 120, 122, 123, and 126 did not record properly. In addition, OBS 124 lost a section of traces at short offsets. The quality of the recorded data is very good, except for the two eastern-most instruments at the Vøring Plateau: OBS 133 has a low signal-to-noise ratio and no arrivals observed at offsets greater than 50-60 km, and OBH 132 has signal only up to 70–80 km offset. We show selected data sets with model fits in Figures 4–8, and all data and models in the supporting information.

Sedimentary refracted arrivals tend to be obscured by earlier refracted basement arrivals, but reflections off top basement give some control on sedimentary velocities. We take the term basement to refer to the igneous crust here. Except for OBS/H 132 and 133, the data have arrivals reflected off the Moho (P_MP), or from diving waves in the lower (P_{g4}) and lowermost crust (P_{g5}). A number of instruments also record arrivals traveling through the uppermost mantle (P_n). Some reflections from middle to lower crustal levels at short offsets were modeled by floating reflectors, and a few late arrivals were modeled by floating reflectors in the mantle. However, such arrivals may have different origins, e.g., they may be out-of-plane reflections or complex multiples.

The westernmost instruments (OBS/H 113-115) recorded P_n phases, which constrain the oceanic crust to a ~4 km igneous thickness here (Figure 4). A combination of P_MP, P_n, P_{g4}, and P_{g5} phases document a rapid increase in crustal thickness into the Vøring Spur (Figures 4–6). OBS 121 (Figure 6) has arrivals up to 160–170 km offsets on both sides, and P_MP combined with P_n phases document crustal thinning on the eastern side of the Vøring Spur. The combination of P_MP phases and lower crustal diving waves require a velocity of ~7.0–7.2 km s^{-1} and a low-velocity gradient in the lowermost crust (Figure 9). Local conditions prevent much energy to enter the P_{g5} phase in the western part of the Vøring Spur. It is very faint on OBS 117 and OBH 118, and long offset arrivals are clearly dominated by Moho reflections and are modeled as

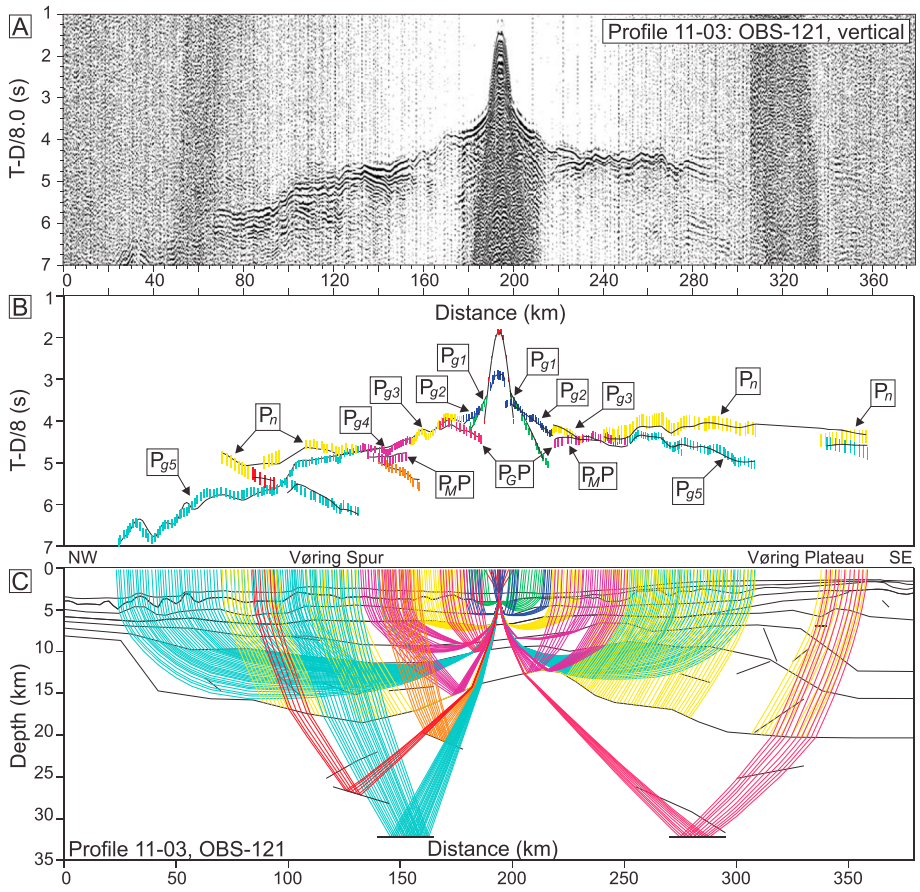

Figure 6. Data, interpretation, and ray tracing of OBS 121, Profile 11-03, Vøring Spur and Plateau. (a) OBS data, vertical component, and offset-dependent scaling. (b) Arrival time interpretation and model reproduction. Phase picks are shown by vertical bars, where the height of the bar shows interpretation uncertainty. Calculated times for each phase are shown by solid black lines. (c) Ray tracing of the velocity model. Ray colors correspond to the pick bar colors in Figure 6b.

such (Figure 5). The P_{g5} phase is also of low amplitude on OBH 114 (Figure 4) for middle parts of the spur, but more seismic energy appears to enter the lowermost crust in the eastern part (Figures 5 and 6).

OBS 121 also gives good constraints on the outer Vøring Plateau. OBS/Hs 124-131 further cover this part of the crust with P_MP and P_{g5} phases (Figures 7 and 8). OBS 124 detect the continent-ocean transition (COT) from the western side (Figure 7). It is seen as a delay of the P_{g5} phase in the east, constraining a drop of seismic velocities at midcrustal levels. This velocity change is also observed on OBS/Hs 125 to 128 (Figure 8). Moho depth of the outer Vøring Plateau is constrained by P_MP phases on OBS 124 (Figure 7), OBS 125, OBH 128 (Figure 8), and OBS 131. OBS 121 (Figure 6) and OBH 130 also have P_n phases, increasing the accuracy of the crustal thickness model of the outer margin.

There is a low-velocity layer below the inner part of the SDR sequence, causing a break between top basement and midcrustal seismic arrivals seen on OBH 130 through OBS 133. These observations are consistent with extrusive magmatic layers deposited on either sedimentary rocks or on low-velocity magmatic rocks just west of the Vøring Escarpment.

3.1. Model Resolution and Sensitivity

Inspecting the ray coverage density (in a 2.5 by 0.25 km distance-depth grid) reveals that the lower crust of the Vøring Spur is better covered than that of the Vøring Plateau (Figure 10a). At the margin, the best coverage is at midcrustal levels. For the spur, the coverage is both more even and better in the lower crust. In order to estimate the quality of constraints for individual velocity nodes, we grid the diagonal values of the resolution matrix for both upper and lower boundary nodes (Figure 10b). The values range from 1 to 0; the latter shows an unconstrained node. A value above 0.5 indicate a reasonably well resolved parameter

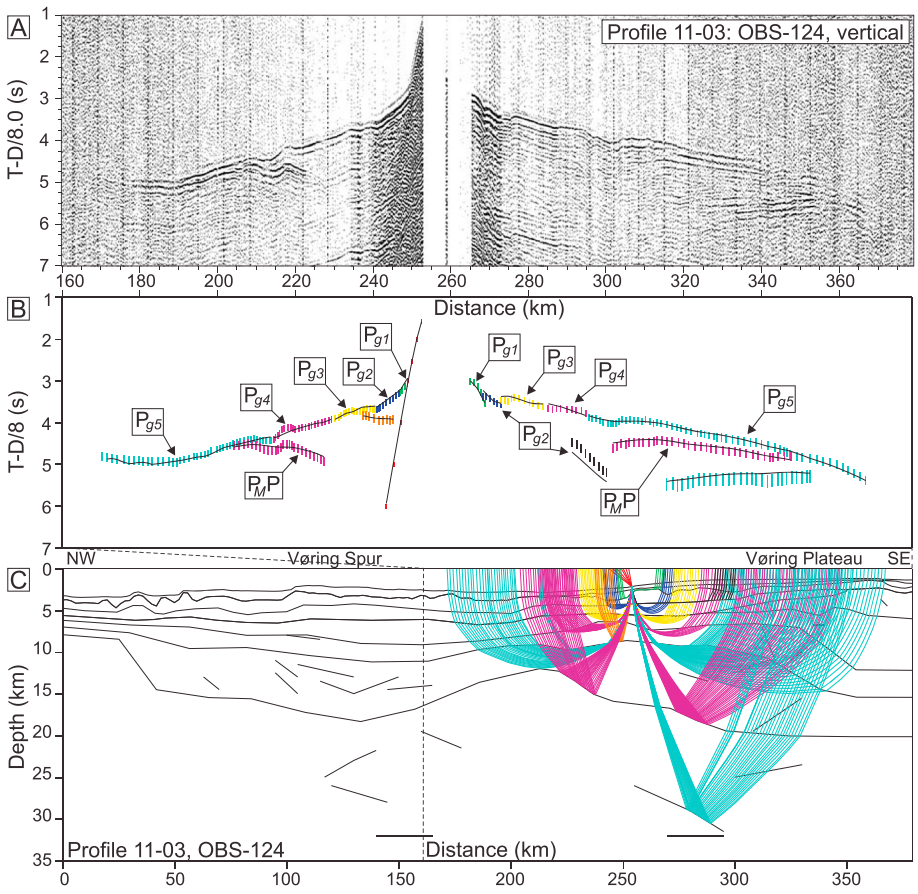

Figure 7. Data, interpretation, and ray tracing of OBS 124, Profile 11-03, Vøring Plateau. (a) OBS data, vertical component, and offset-dependent scaling. (b) Arrival time interpretation and model reproduction. Phase picks are shown by vertical bars, where the height of the bar shows interpretation uncertainty. Calculated times for each phase are shown by solid black lines. (c) Ray tracing of the velocity model. Ray colors correspond to the pick bar colors in Figure 7b.

[*Zelt and Smith*, 1992]. The analysis is based on both reflected and refracted phases, since reflections play an important role in constraining the lower crust. However, the sedimentary layers are only constrained by a few reflections from the top of the oceanic crust, and the resolution is therefore low. Upper crustal velocities are constrained by short offset refracted arrivals, with less illumination from different stations than deeper nodes, and appear to be only moderately resolved. Lower crustal velocity nodes of the Vøring Spur have a resolution of 0.7–0.8 in the top of the layer, while bottom layer nodes have values of 0.5–0.6, and are very well constrained. Lower crustal velocity top layer nodes of the outer Vøring Plateau have values around 0.6 and are well constrained, though bottom layer nodes are less well constrained here.

The fit statistics for the most important phases are shown in Table 1. The RMS Δt difference between interpreted and calculated traveltimes range from 52 ms for the direct water arrival, to 90 ms for the P_n phase. The χ^2 value based on the interpretation uncertainty for all phases is below 1. This indicates that the model can be slightly changed and still produce a fit within interpretation uncertainty, which constrain model sensitivity. To quantify that, we ran an automated search through a range of selected velocity and depth nodes. Since we study the lower crust of the oceanic domain to estimate the degree of mantle melting, this part of the model was targeted. Due to the trade-off between velocity and depth, we ran through the depth nodes of the Moho, and the bulk lower crustal and upper mantle velocity (using P_{g5}, P_MP, and P_n phases) to estimate minimum and maximum velocity models. Chosen depth nodes were changed in the same direction by 0.1 km, and the velocity nodes were then cycled through a predefined interval at 0.01 km s^{-1} steps. Each model was ray traced and fit statistics extracted. The procedure was repeated until the depth nodes had cycled through the chosen interval.

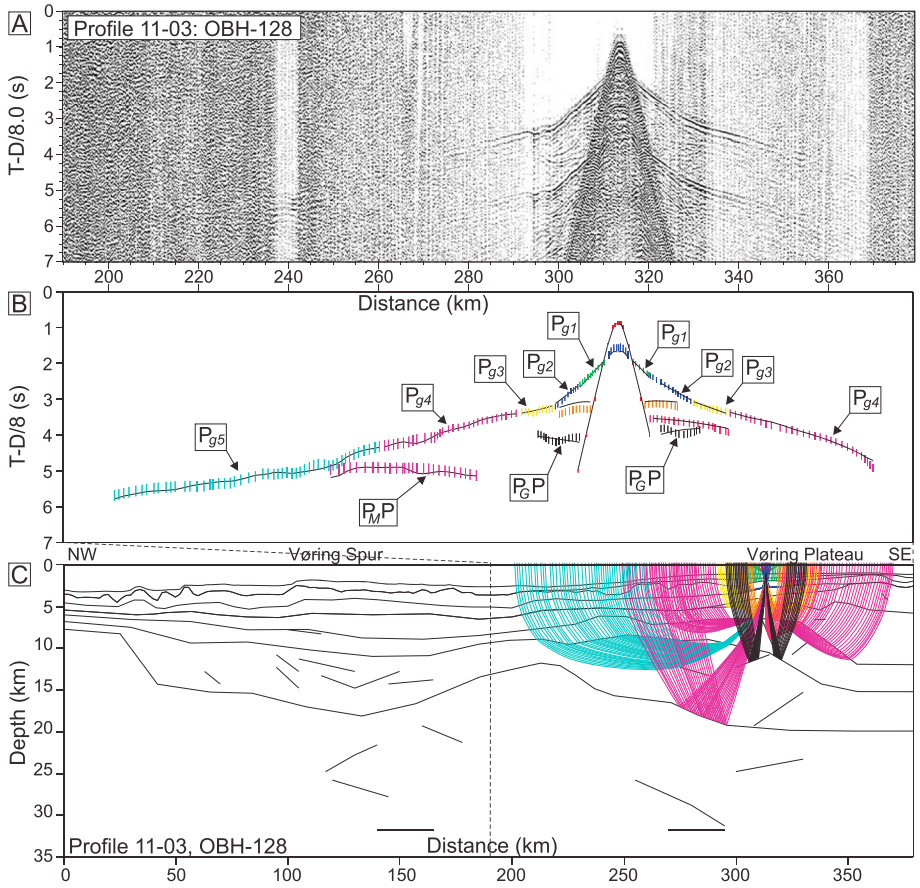

Figure 8. Data, interpretation, and ray tracing of OBH 128, Profile 11-03, Vøring Plateau. (a) Hydrophone data and offset-dependent scaling. (b) Arrival time interpretation and model reproduction. Phase picks are shown by vertical bars, where the height of the bar shows interpretation uncertainty. Calculated times for each phase are shown by solid black lines. (c) Ray tracing of the velocity model. Ray colors correspond to the pick bar colors in Figure 8b.

For the Vøring Spur 1681 different models were run for nodes between 40 and 201 km. The same number of models was run for the Vøring Plateau for nodes between 225 and 340 km. The results are summarized in Figure 11, showing contoured χ^2 and RMS Δt fit. Also, the ability of the model to trace rays to all observed offsets limits the model space. Increasing loss of rays is indicated by increasingly dark gray shading. Based on models with $\chi^2 < 1$ we estimate model uncertainty at the Vøring Plateau to be −1.9/1.7 km for the Moho depth and −0.13/0.10 km s^{-1} for the bulk lower crustal velocity. For the Vøring Spur, it is −1.3/1.0 km for the Moho depth and ±0.08 km s^{-1} for the lower crustal velocity, confirming that this is the best constrained part of the model.

4. Discussion

4.1. Crustal Nature From Velocity

One of the possible origins of the Vøring Spur considered was that it could be a continental fragment. The velocity model shows lower crustal velocities of 7–7.2 km s^{-1} for the Vøring Spur, consistent with a gabbroic composition [e.g., *Christensen and Mooney*, 1995]. To compare regions of different nature, we extract 1-D velocity profiles from Profile 11-03, and from other OBS profiles. Ocean and sediments were removed by setting the top to the first layer having a velocity above 3 km s^{-1}. In Figure 12a we compare a typical 1-D velocity profile from the Vøring Spur to a 1-D profile from the outer margin, to show the similarity (locations in Figures 1 and 13). The oceanic nature of the outer Vøring Plateau here is confirmed by comparing to a 1-D profile extracted from Profile 10-03 farther north, where magnetic seafloor spreading anomalies are identified [*Breivik et al.*, 2009] (Figure 13). We also compare to the Jan Mayen microcontinent to test how a continental fragment could look like if it was present. Two 1-D transects were extracted from the top of the Jan Mayen Ridge [*Breivik et al.*, 2012; *Kodaira et al.*, 1998] (locations in Figure 1), and they show a

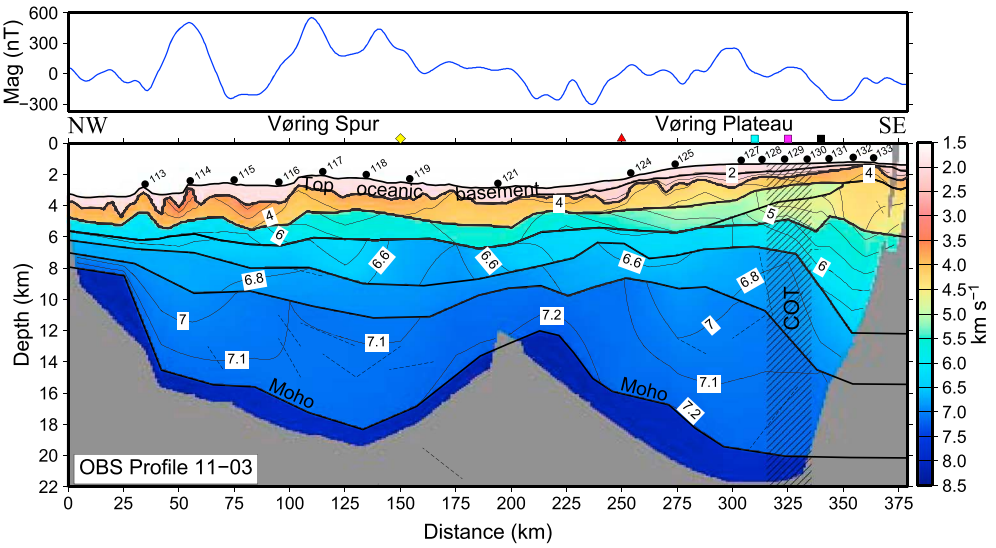

Figure 9. Gridded crustal velocity model of Profile 11-03. See Figure 2 for location. The parts of the model not covered by rays are masked; floating reflectors (dashed lines) do not constrain velocity and are not included in the ray coverage. The OBS/H locations are numbered on the seafloor. Hachures indicate the continent-ocean transition (COT). Velocity contour interval is 0.2 km s^{-1}, except for the lowermost crustal layer where it is 0.1 km s^{-1}. Positions of 1-D velocity profiles shown in Figure 12 are indicated by their respective color symbols. The magnetic track collected along profile is shown above.

significantly lower velocity through the whole crust. Thus, the velocity structure gives no indication of continental material within the spur.

The COT is interpreted to between 315 and 335 km in the model (Figure 9), where there is a rapid fall in mid-crustal velocities. In Figure 12b we compare a 1-D velocity profile from the COT to profiles located on either side (locations in Figures 1 and 13). At 310 km, the velocity is very similar to that of the outer Vøring Plateau (Figure 12a), but with a greater crustal thickness. At 340 km, the velocity is similar to those seen on the Jan Mayen microcontinent (Figure 12a), but with lower crustal velocity similar to that of the adjacent oceanic crust. This high-velocity layer is commonly seen below the continental crust of the Vøring Plateau and has been interpreted as magmatic underplating or lower crustal intrusive complexes related to the breakup magmatism [e.g.,*Mjelde et al.*, 2001]. Profile 11-03 does not constrain this layer very well. The 1-D profile at 325 km from the middle of the COT shows intermediate velocities. The narrow transition to continental crust is similar to profiles to the north and south [*Breivik et al.*, 2006, 2009; *Mjelde et al.*, 2001, 2005], indicating moderate extension of the continent during breakup, as first noted by *Mutter and Zehnder* [1988].

4.2. Constraints on Mantle Melting Degree

In order to produce the thick oceanic crust observed at the margin, the mantle must either undergo a high degree of melting, or more mantle rocks must be fluxed through the melting region. The results of the melting process can be observed in the geochemical composition of the rocks. Increasing melt degree caused by elevated temperature increases the MgO content in relation to the FeO content [*Klein and Langmuir*, 1987; *McKenzie and Bickle*, 1988]. Compositional variations relate to the physical properties of rocks and can, in principle, be measured using seismic velocity data.

A high melt degree causing elevated MgO content will result in higher seismic velocities [*White*, 1989; *Kelemen and Holbrook*, 1995; *Korenaga et al.*, 2002]. If the volcanic margin was created by transient elevated mantle temperature as expected from a mantle plume model, there will be a positive correlation between igneous crustal thickness (H) and mantle melt degree and therefore also with seismic velocity (V_p) [*Holbrook et al.*, 2001]. Other models for excess magmatism predict other H-V_p correlations: Small-scale convection fluxes more mantle material through the melt zone than passive seafloor spreading [*Mutter et al.*, 1988; *Boutillier and Keen*, 1999], resulting in a low H-V_p correlation. Since the mantle melt degree then changes little with change in magma production, composition and V_p remain more uniform over a wide range of crustal thickness. Mantle enriched in fusible components will produce a negative H-V_p correlation [*Holbrook et al.*, 2001; *Korenaga et al.*, 2002; *Parkin and White*, 2008; *Sallarès et al.*, 2003, 2005].

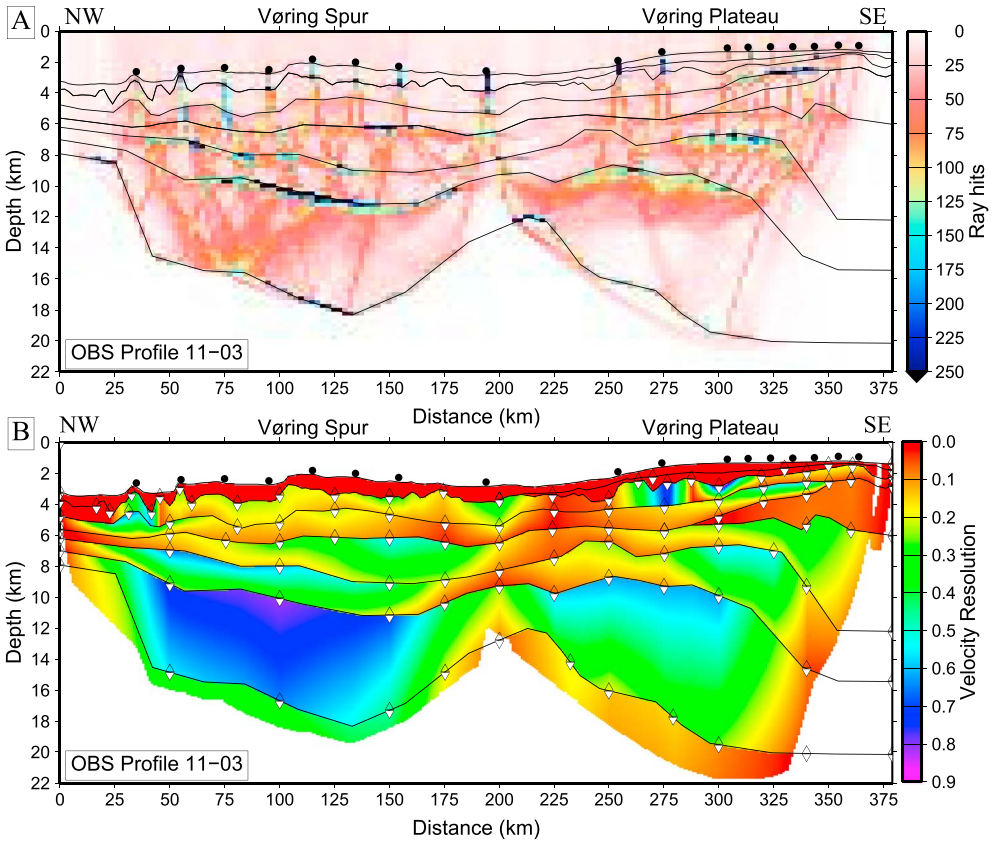

Figure 10. Ray coverage and velocity node resolution. (a) Gridded ray coverage of the Profile 11-03 velocity model, excluding floating reflectors. The binning is 2.5 km horizontally and 0.25 km with depth. (b) Gridded resolution parameters of the *P* wave velocity nodes obtained from inversion, omitting the water layer. Velocity nodes in the top and bottom of the layers are shown in white inverted triangles and transparent triangles, respectively.

A number of studies estimate the mantle melting process during breakup in the NE Atlantic [*Holbrook et al.*, 2001; *Parkin and White*, 2008; *White et al.*, 2008; *Breivik et al.*, 2009, 2012]. While results are consistent with temperature-driven excess melting, systematic variations between margin segments are also emerging. *Holbrook et al.* [2001] showed that a passive upwelling mantle with elevated temperature could account for the breakup magmatism at Southeast Greenland. A conjugate Hatton Bank profile similarly indicates a passive, temperature-driven mantle melting [*Parkin and White*, 2008; *White et al.*, 2008]. On the other hand, active upwelling appears important closer to the GIR in addition to elevated temperature, where both effects were attributed to the Iceland mantle plume [*Holbrook et al.*, 2001].

The Norway Basin conjugate margins have also been studied in recent years. A profile over the Faeroes margin produced results similar to that of the Hatton Bank [*Parkin and White*, 2008; *White et al.*, 2008]. Farther north on the Møre Margin, the magma productivity was lower [*Breivik et al.*, 2006], indicating little or no active upwelling [*Breivik et al.*, 2009]. Similarly, two profiles over the conjugate volcanic margin of the Jan Mayen microcontinent show passive mantle upwelling and a fall in mantle temperature and magma production toward the north [*Breivik et al.*, 2012].

Since the breakup magmatism did fall off northward along the Møre Margin, one should expect that this marked the extent of the plume influence. However, magmatism increased greatly north of the transform margin offset to the Vøring Plateau [*Berndt et al.*, 2001; *Mjelde et al.*, 2005; *Breivik et al.*, 2009]. It is also high on the conjugate Northeast Greenland Margin [*Voss and Jokat*, 2007]. Earlier results showed a complex H-V_p relationship for Profile 10-03 [*Breivik et al.*, 2009] resembling results close to the GIR where both active upwelling and elevated temperature appear to have been present [*Holbrook et al.*, 2001]. Thus, a secondary process like small-scale convection may explain why this increase in magmatism occurs. To further explore

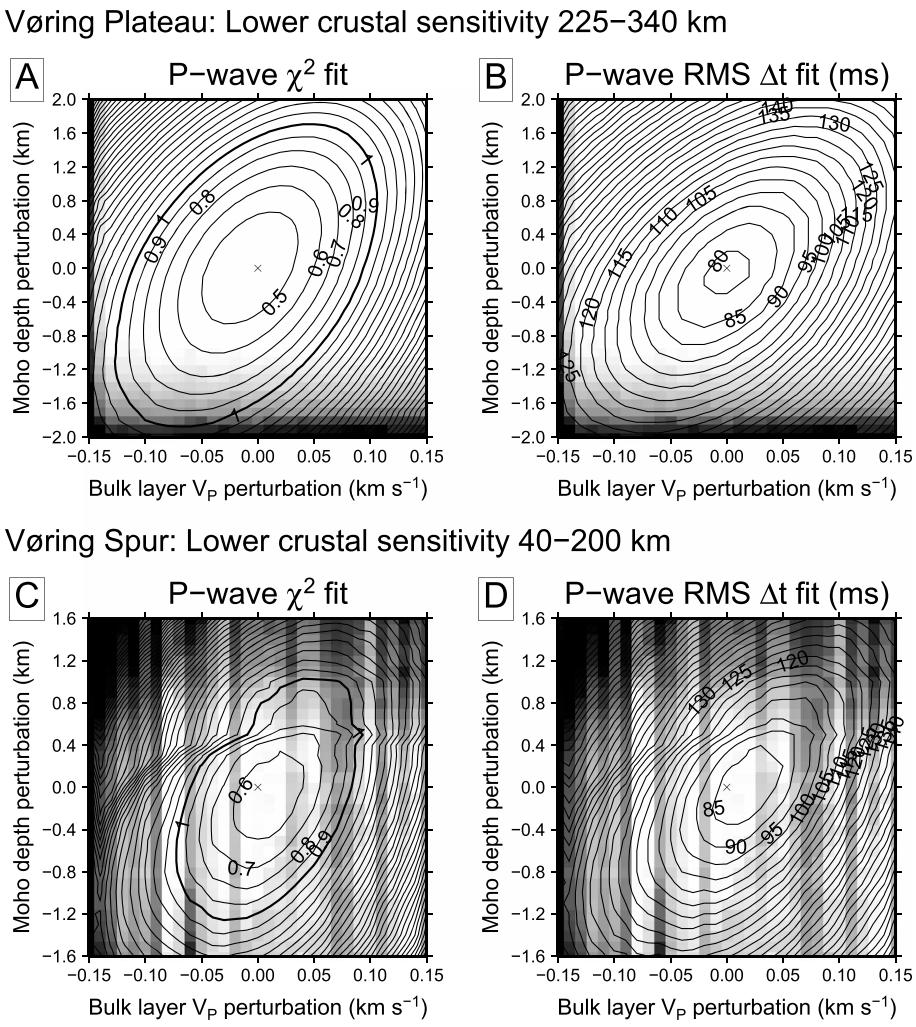

Figure 11. Profile 11-03 *P* wave model sensitivity to lower crustal velocity changes against Moho depth based on P_{g5}, P_MP, and P_n phases. (a and b) Model sensitivity for the outer Vøring Plateau; (c and d) model sensitivity for the Vøring Spur. Background shading indicates the ability of the model to trace arrivals to all observed locations. The shading starts at 2% loss and reaches black at 10% loss.

this, we analyze the H-V_p relationships of Profile 11-03 in the south and that of the adjacent older Profile 1-99 [*Mjelde et al.*, 2005] (Figure 2).

4.3. H-V_p Analysis of the Vøring Margin

Crustal thickness is easily measured, but the velocity must be corrected to standard conditions. In situ velocity depends both on pressure and on temperature [*Fountain and Christensen*, 1989]. *Holbrook et al.* [2001] adjust observed values to a reference pressure of 600 MPa and a temperature of 400°C, using 0.00022 km s^{-1} MPa^{-1} and −0.0005 km s^{-1} $°C^{-1}$. Pressure is estimated by converting velocity to density [*Ludwig et al.*, 1970], and the weight of the overlying column can then be calculated. Temperature is estimated by using a linear temperature gradient from 10°C at the seafloor to 750°C at 40 km depth. Grid cells with upper crustal velocity below 6.85 km s^{-1} are assigned 6.85 km s^{-1} before correction in order to eliminate the effect of porosity [e.g., *Wilkens et al.*, 1991; *Jacobson*, 1992]. After estimating the in situ conditions, the velocity of each cell of the gridded velocity models can be corrected. The average velocity can then be calculated for columns and correlated with crustal thickness. Corrected average velocities will differ slightly from the measured in situ velocities of Figure 9.

Not all studies use the corrections outlined above. *Parkin and White* [2008] and *White et al.* [2008] refer to conditions of 230 MPa and 150°C, which is close to lower crustal conditions on the NE Atlantic margins; therefore, the in situ velocity was not further corrected. They only include lower crust with velocity higher

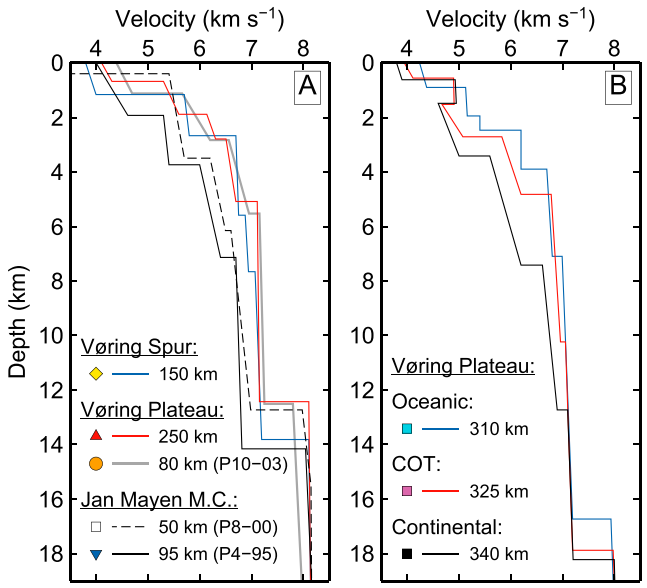

Figure 12. Profile 11-03 1-D velocity profiles compared between zones, to the northern Vøring Plateau, and to the Jan Mayen microcontinent. Zero depth is adjusted to the top of the first layer with velocity exceeding 3 km s^{-1}. Kilometer values indicate 1-D positions along the modeled profiles. Color symbols refer to positions in Figures 1, 2, 9, and 13. (a) Typical Vøring Spur velocities are similar to that of the outer Vøring Plateau but higher than velocities of the Jan Mayen microcontinent from OBS Profile 8-00 [*Breivik et al.*, 2012] and from OBS Profile 4-95 [*Kodaira et al.*, 1998]. Outer Vøring Plateau velocities are also compared to a 1-D velocity profile from Profile 10-03 farther north on the plateau, at seafloor spreading anomaly 23. (b) Defining the continent-ocean transition (COT). The COT 1-D profile is in the middle of the hachured region at 325 km from Figure 9. The 1-D profile located 15 km seaward of that is similar to the outer margin and the Vøring Spur as seen in Figure 12a. Lower midcrustal velocities comparable to the Jan Mayen continental crust are found 15 km landward of the COT 1-D profile.

than 6.7 km s^{-1}. *Breivik et al.* [2012] compared the two different approaches. Using *Holbrook et al.* [2001] corrections placed our Jan Mayen margin data somewhat low in the diagram, tending toward indicating active upwelling. The *Parkin and White* [2008] and *White et al.* [2008] approach predicted normal seafloor spreading better and placed the data closer to passive upwelling, but it is also more sensitive to lower crustal velocity variations. We have had the opportunity to test the iSIMM Faeroes profile [*White et al.*, 2008], and both approaches reproduced the published results.

In Figure 14, we have used the *Holbrook et al.* [2001] corrections to compare Profiles 10-03, 11-03, and 1-99. The H-V_p data are extracted up to the outer edge of the estimated COT taken from *Breivik et al.* [2009], *Mjelde et al.* [2005], and this work. It does not pinpoint the line of breakup, but it makes it reasonable to assume that we are over oceanic crust for the analysis. Still, one should be careful to interpret process from the results near the COT, as there will be some velocity smearing over a potentially sharp continent-ocean boundary due to limited horizontal resolution of the seismic experiments [e.g., *Roberts et al.*, 2009]. Landward, there is a strong negative H-V_p correlation due to the increasing presence of continental crust, not shown here. Profile 11-03 shows a transition from a lower to a higher velocity with abating magma production in the H-V_p diagram, similar to what is observed on Profile 10-03. The figure also shows curves calculated from minimum and maximum models indicated by the sensitivity analysis (Figure 11). For Profile 1-99 the curve is derived from the published model [*Mjelde et al.*, 2005], which has no sensitivity analysis. This profile from the central Vøring margin shows higher crustal thickness, higher V_p, and a positive H-V_p correlation. The results are below the passive-upwelling curve in the diagram, except for a strong V_p spike occurring around 15 km crustal thickness.

The V_p results for the profiles are also shown as a function of time (Figure 14). For Profile 10-03, the seafloor spreading history is well constrained, and an accurate time-dependent V_p curve can be obtained. However, central and southern parts of the Vøring Plateau show a chaotic magnetic anomaly pattern (Figure 13). If the magmatism is not confined to the spreading axis, large lava flow distances will result in magnetic anomalies that cannot be used for dating [*Smallwood and White*, 2002]. Some anomalies clearly correlate with the bottom of the margin slope, showing that they do relate to large flows (Figure 13). Profile 1-99 reaches seafloor spreading anomaly 22 just before the anomaly starts to follow the foot of the margin slope. Applying the spreading model of Profile 10-03 [*Breivik et al.*, 2009] from anomaly 22, the V_p versus time development can be calculated (Figure 14). Profile 11-03 is more challenging, as the magnetic anomalies are chaotic both over the margin and the Vøring Spur. Anomaly 22 was extrapolated along the seafloor anomaly trend from the northeast to the 160 km position in the model, and the spreading calculated from there.

The results show common characteristics for the temporal development of the breakup magmatism from different parts of the Vøring Plateau (Figure 14, right column): The slightly negative H-V_p correlation for the

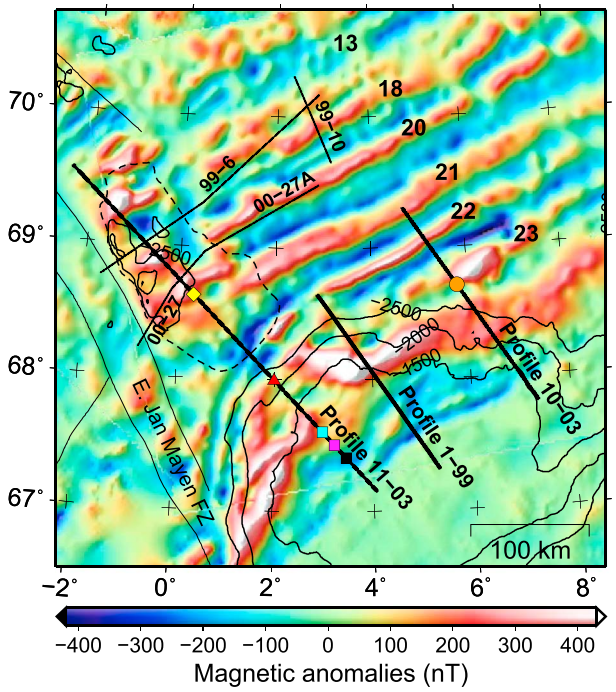

Figure 13. Magnetic map over the study area with OBS survey navigation, illuminated from the NW. The central part of the map is covered by the newer surveys RAS-03 and JAS-05 [*Olesen et al.*, 2007; *Gernigon et al.*, 2009], and marginal parts by the compilation of *Verhoef et al.* [1996]. Some bathymetric contours and the extent of thick oceanic crust (dashed line) under the Vøring Spur [*Breivik et al.*, 2008] are shown, and seafloor spreading anomalies are annotated. (Approximate ages: A23: 51.4 Ma, A22: 49.4 Ma, A21: 47.1 Ma, A20: 43.2 Ma, A18: 39.3 Ma, and A13: 33.3 Ma [*Cande and Kent*, 1995].) The positions of the MCS lines in Figure 16 are shown by thin black lines. Positions of 1-D velocity profiles shown in Figure 12 are indicated by color symbols.

first 0.4–0.5 Ma could indicate the presence of continental material farther out than the interpreted COT, but it is more likely caused by the expected lateral velocity smearing. Crustal breakup between Norway and Greenland is believed to be complete during magnetic Chron 24R, making it older than ~53.4 Ma [e.g., *Hinz et al.*, 1993; *Mosar et al.*, 2002]. The next section shows a positive H-V_p correlation starting at somewhere between 53.5 Ma and 52.7 Ma and lasting for 1–1.5 Ma. The curves are below the passive mantle upwelling line in Figure 14.

Since the correlation is positive, it suggests a cooling mantle reservoir, causing a reduction of the mantle melt degree with time. If this is combined with active upwelling, which in itself would produce low correlation, that could explain the results up to 51.5–52 Ma. The mantle melt degree and therefore the MgO content would be less than expected from the crustal thickness, while retaining the signature of a cooling mantle source. This is essentially the model *Holbrook et al.* [2001] used to explain similar results near the GIR at the East Greenland Margin.

There is a subsequent transition to higher average velocity, peaking at about 51.5 Ma, where elevated mantle temperature alone can account for the 10–15 km thick igneous crust produced. After that, there is again a positive H-V_p correlation toward normal seafloor spreading, consistent with a cooling mantle source. Active upwelling or other effects are less likely to have played a role at this stage. At Profile 11-03, the velocity increase at 50 Ma is not seen on Profile 10-03 and is related to the Vøring Spur development.

Breivik et al. [2012] showed that the two different approaches on how to average the velocity produce somewhat different temperature estimates for the mantle anomaly at breakup for the East Jan Mayen microcontinent volcanic margin. The *Holbrook et al.* [2001] approach gives the highest estimate, but is inconsistent in indicating an exceptionally cool background mantle, not seen when applied to the iSIMM Faeroes profile. Relative differences and trends should be more reliable than absolute temperature. For the Vøring margin, our studies indicate a temperature anomaly of 80–150°C, lowest in the south, comparable to observations on the Southeast Greenland Margin [*Holbrook et al.*, 2001], the Faeroes Margin [*Parkin and White*, 2008; *White et al.*, 2008], and the Southeast Jan Mayen microcontinent margin [*Breivik et al.*, 2012]. It is probably less than 50°C for the Møre and Northeast Jan Mayen margins. We expect conclusions on processes derived from trends to be robust. Results appear to be largely consistent between different surveys and research groups, and on conjugate margins.

The observed double peak in the temporal development of lower crustal seismic velocity on this margin segment must relate to the processes governing magmatism here. Preexisting lithospheric structure should affect the distribution of plume material. *Armitage et al.* [2010] modeled this possibility for the Hatton Bank Margin and predicted both increased magmatism and a double peak in the lower crustal seismic velocity temporal development, though the results are highly sensitive to spreading rate. Their fast-spreading model shows a time interval of ~3.5 Ma between the peaks, and amplitude of ~0.1 km s^{-1}, which compares

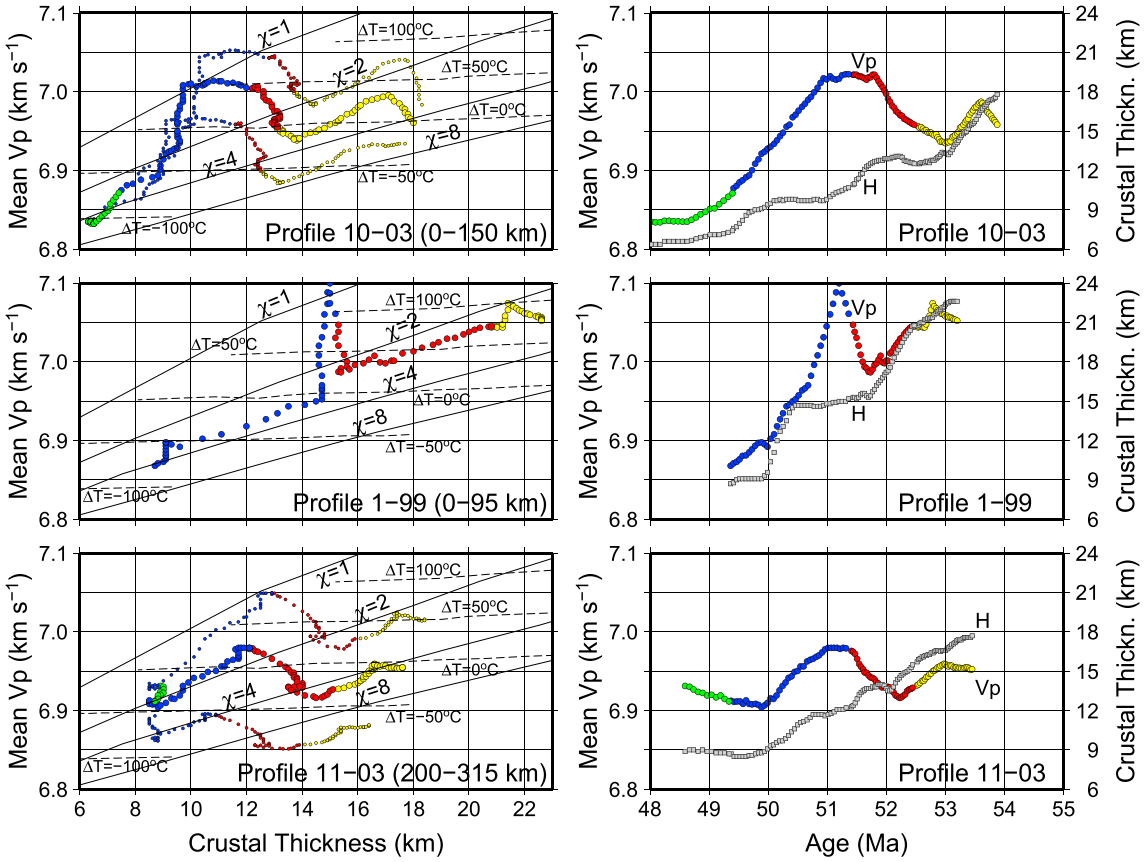

Figure 14. (left column) Crustal thickness variations plotted against mean V_P of the igneous crust for Profile 11-03, Profile 1-99, and Profile 10-03, using the *Holbrook et al.* [2001] corrections. Sampling interval is 1 km horizontally. The mantle melting curves indicate the degree of active upwelling (χ = 1 is passive), while ΔT shows deviation from a normal potential mantle temperature of 1280°C. Small symbols indicate minimum and maximum velocity models. (right column) The same data plotted against age for Profile 11-03, Profile 1-99, and Profile 10-03. Crustal thickness (*H*) is shown by gray squares, while mean velocity (V_P) is shown by color-filled circles. Colors indicate position relative to magnetic seafloor spreading anomalies (Figure 14, left and right columns). Yellow: from COT to A24a, red: A24a to A23, blue: A23 to A22, and green: A22 to A21.

well with the 2–2.5 Ma interval and 0.07–0.1 km s^{-1} amplitude observed at the Vøring Plateau. However, a double peak is actually not observed at the Hatton Bank, for which the model was designed. Rifting is Late Cretaceous at the Hatton Basin, while it is Late Jurassic to Early Cretaceous at the Vøring and Møre basins [*Brekke*, 2000]. Thus, the effect should be greater at the Hatton Bank since the lithosphere has had less time to readjust. The moderate magmatism observed at the Northern Møre Margin [*Breivik et al.*, 2006] further complicates this scenario. Clearly, there is still a lot to be learnt about the breakup magmatism. Early deep sea drilling sampled igneous rocks at the Vøring margin, but the boreholes are either placed over the continent-ocean transition zone, or near the foot of the margin slope, and missed the region where the greatest changes occur [e.g., *Breivik et al.*, 2009; *Zehnder et al.*, 1990]. The Vøring Plateau could be a prime location to test the importance of different mantle melting processes geochemically through new drilling.

4.4. *H*-V_p Analysis of the Vøring Spur

Analyzing the profile between 40 and 200 km shows that there is a low correlation between crustal thickness and velocity (Figure 15). The *H*-V_p curve is remarkably flat between 8 and 15 km crustal thickness, with the velocity only dropping slightly in the westernmost flank of the high. The crustal composition clearly does not vary significantly with crustal thickness change, and thus, the melting degree of the mantle that supplied magma to different parts of the crust did vary little. This shows that the thick crust is not related to the breakup magmatism, as proposed by *Gernigon et al.* [2009]. If all crustal thickness was created at the spreading ridge, it could be interpreted as the result of increased magmatism due to small-scale convection. As *Breivik et al.* [2008] showed, there is extensive later uplift of the high. It was concluded that the uplift had

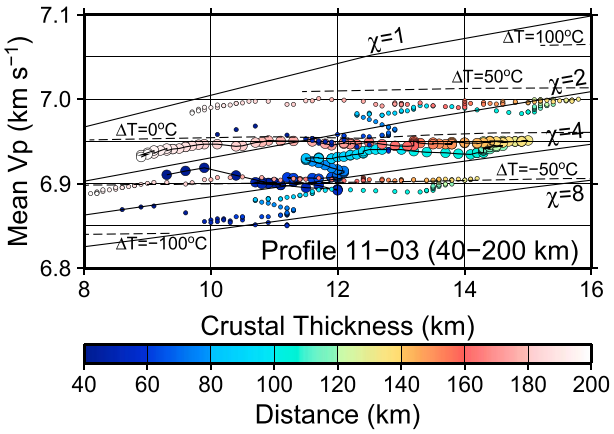

Figure 15. Crustal thickness variations plotted against mean V_P for the Vøring Spur from Profile 11-03, based on the corrections of *Holbrook et al.* [2001]. Small symbols indicate minimum and maximum velocity models derived from Figure 11. Color codes show position along model. Other symbols are as in Figure 14.

to be caused by secondary magmatic growth of the oceanic crust. Two separate melting events would both experience a moderate mantle melting, and the observed lack of a clear *H*-V_p trend is consistent with this.

The location of the Vøring Spur at the tip of the Aegir Ridge is conspicuous. In an attempt to explain that, *Breivik et al.* [2008] proposed that magmatism could originate from the deepest remnant of the Aegir Ridge melting not extracted before the cessation of the seafloor spreading subsequently carried northeast with the asthenospheric flow from the Iceland plume. The justification for the model is that young oceanic asthenosphere is a distinct seismic low-velocity zone, believed to be caused by the presence of a small melt fraction [e.g., *Schmerr*, 2012]. While others have argued that changing physical properties of the solid phase immediately below the solidus could explain this [e.g., *Stixrude and Lithgow-Bertelloni*, 2005], magnetotelluric data support the presence of a melt fraction under the East Pacific spreading ridge [*Key et al.*, 2013], and at 45 to 70 km depth beneath 20 Ma old oceanic lithosphere near a subduction zone in the East Pacific [*Naif et al.*, 2013]. Partial melts are stable at those depths in a warm and damp mantle [*Hirschmann*, 2010]. The asthenosphere is hotter and shallower beneath a recently active spreading axis like the Aegir Ridge, favoring preservation of a small melt fraction. The magma emplacement model relied on the assumption that bottom lithospheric topography could guide asthenospheric flow generated by the Iceland Plume along the Aegir Ridge trend to the Vøring Spur location. Also, when asthenosphere flows into the Norway Basin area it would meet a thinner lithosphere, and mantle melting through ascent could possibly occur and replenish a small melt fraction under the central parts. A recent seamount is observed at the Aegir Ridge, though magmatism indicating strong interaction with bottom lithosphere topography in the area is absent [*Breivik et al.*, 2008]. Asthenospheric flow northward across the East Jan Mayen Fracture Zone (EJMFZ) will encounter a thicker lithosphere at the Vøring Spur location, and melting through mantle ascent there is not expected. Thus, a mechanism to extract an already present melt fraction transported there is needed. The asthenosphere would experience shear due to the step in lithospheric thickness across the fracture zone, and shear deformation of a rock with a small melt fraction is shown to be efficient in mobilizing and extracting melt [e.g., *Kohlstedt and Holtzman*, 2009]. Underplating through this mechanism would produce the observed *H*-V_p correlation, since the extracted melt is from low-degree mantle melting. This is currently not a well explored model, and other processes could be at work. However, the uncertainty concerning mechanism does not invalidate the conclusion that the Vøring Spur was created by rejuvenated magmatism.

4.5. Dating the Vøring Spur Formation

There are two alternative ages for the formation of the Vøring Spur published. *Gernigon et al.* [2009] argued that the high formed at a triple junction, implying that it is of Early Eocene age. However, disturbance of the sedimentary pattern around the Vøring Spur led *Breivik et al.* [2008] to conclude that the bathymetric high is younger than the 47 to 33 Ma old seafloor it rests on (Figure 13) and that it was formed mostly during the Late Miocene.

Early sedimentation on top of the high was substantial, while later sedimentation only onlaps the flanks. There is a prominent unconformity between these two sequences off the high. *Hjelstuen et al.* [2007] show that the upper sequence is mostly distal turbidites driven by Plio-Pleistocene glaciations of the Barents Sea, 2.6 Ma and younger, dating the unconformity to the Late Pliocene. The Late Miocene dating of *Breivik et al.* [2008] therefore appears too old. We suggest that a dating near the Late Miocene/Pliocene boundary may be reasonable, as some movement also occurred below this unconformity, as shown below.

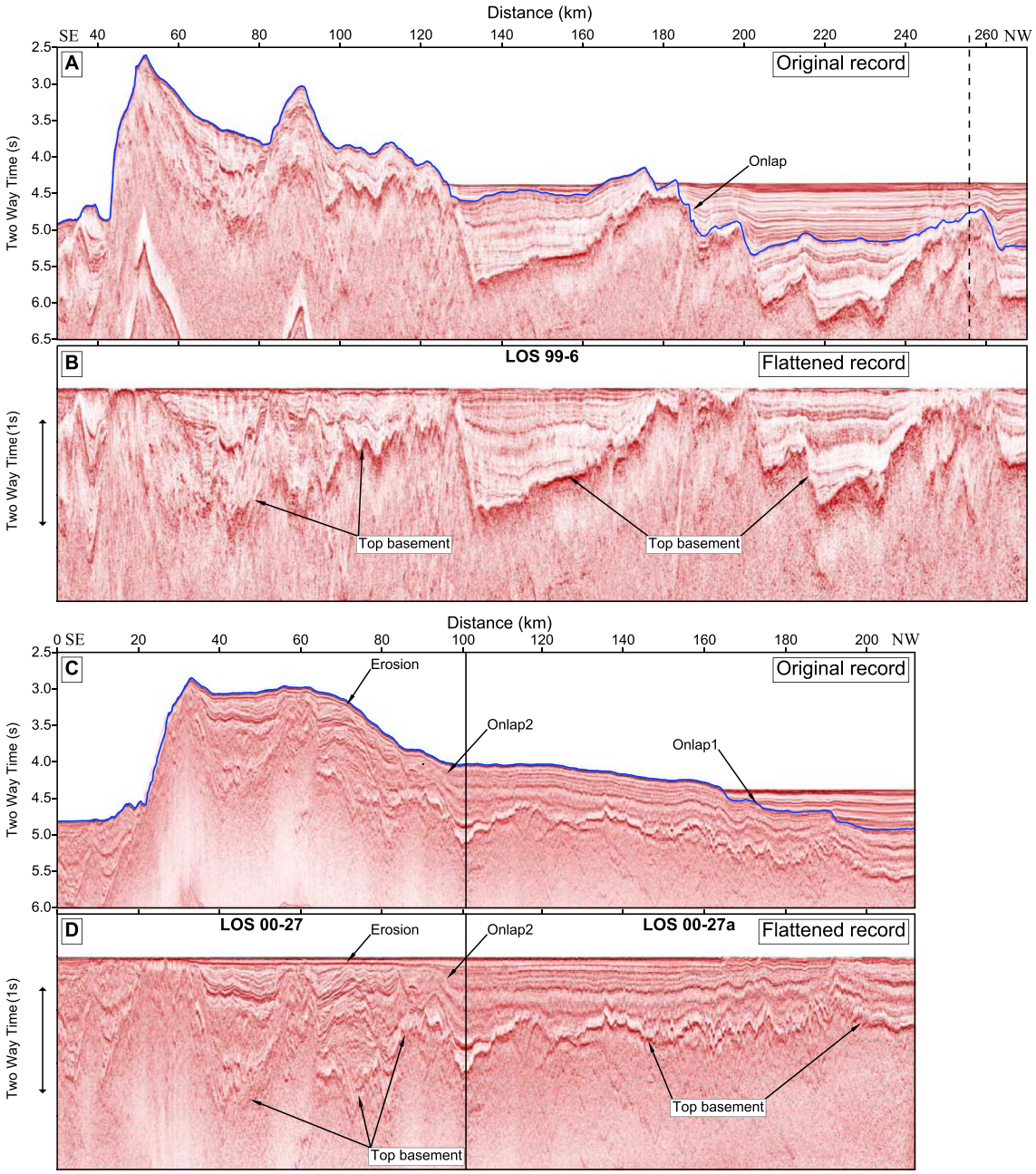

Figure 16. Sediment deposition pattern over and around the Vøring Spur. The main unconformity associated with uplift of the high is indicated by blue lines, extended along bathymetry over the high, used to reconstruct preuplift geometry. Locations are shown in Figures 2 and 13. (a) LOS 99-6, tie to LOS 99-10 (Figure 17) is shown by dashed line. (b) LOS 99-6 flattened on seafloor/unconformity. (c) LOS 00-27/27a composite line showing the sedimentation pattern along a seafloor lineation from where it is buried in the basin to become exposed in the Vøring Spur. (d) Flattened on seafloor/unconformity (Onlap1). Onlap within the deepest sedimentary section (Onlap2) shows an earlier inversion event. Some early erosion of sediments can be seen on the northern flank of the Vøring Spur.

Time flattening can be used to explore the situation before the high was uplifted. Two multichannel reflection seismic profiles crossing the Vøring Spur were flattened either on the main sequence boundary or on the bathymetry over the high where the youngest sequence is absent. After flattening of line LOS 99-6, the sediment package over the high resembles that of the area northeast of it (Figures 16a and 16b). The basement topography with asymmetric depocenters is very similar from the high to surrounding areas. On the composite line LOS 00-27/27a (Figures 16c and 16d), the sediment thickness over the high is comparable to that of LOS 99-6 (Figures 16a and 16b). Sediment thickness is reduced to the half northeast of the high, showing that this part of the high was a local depocenter. An earlier uplift phase is also apparent within the

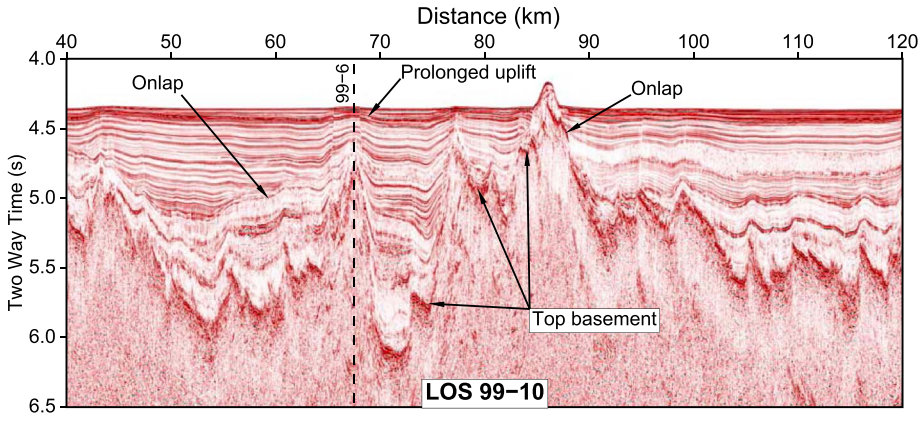

Figure 17. Part of LOS line 99-10 showing sedimentation pattern around the seafloor lineation. Tie to LOS 99-10 (Figure 16a) is shown by dashed line. The location is shown in Figures 2 and 13.

older sequence (Onlap2 in Figures 16c and 16d), with some erosion of the flank of the early high. The relief was moderate, as the younger sedimentary layer transgresses the high. The event thus appears smaller and less extensive than the later uplift, and an accurate dating is presently not possible.

The single-channel reflection data along the OBS profile shows a radical change in the seismic stratigraphy from the Vøring Plateau to the Spur (Figure 3). Early sedimentation filled in rough basement topography on the margin, with a gently draped stratigraphic sequence and a smooth seafloor above. Over the spur, the sedimentation pattern follows the basement topography to a large extent up to the seafloor, which is very rough. This is consistent with a late inversion of a substantial sedimentary package.

Side scan bathymetry (Figure 2) shows conspicuous NE-ENE trending lineaments off the high. LOS line 99-10 crosses one lineament 150 km NE of the main high (Figure 17), revealing a basement ridge with a sedimentary section on top. The line crosses line 99-6 (Figure 16a), showing that the abyssal hill is narrow and elongated in the NE direction. Figure 17 also shows that uplift continued throughout the Plio-Pleistocene. Line LOS 00-27A lies on top of one lineament (Figure 16c), showing that the sedimentary layers are continuous from the deep oceanic basin to the top of the Vøring Spur. The trend of the lineaments follows the magnetic anomalies of the oceanic basement, and they have the shape and dimension of abyssal hills typical for the central and NE Atlantic [*Escartin et al.*, 2008; *Bruvoll et al.*, 2009]. They thus appear to represent uplift or reactivation of the preexisting oceanic crustal fabric.

To explain the large amounts of sediment over the high, *Gernigon et al.* [2009] argued that the Vøring Spur is covered by contourites, transported there by ocean currents. The documented contourite deposits off mid-Norway are, however, of a much lesser magnitude, seen at the footslopes of the margin, or infilling submarine slide scars [e.g., *Laberg et al.*, 2001, 2005]. Contourite deposits often show onlap, sedimentary waves, and other indicators of transport direction, as well as erosion [e.g., *Faugères et al.*, 1999; *Stow et al.*, 2002; *Laberg et al.*, 2005]. We have not observed these typical contourite features on the available data. Any depositional model for the Vøring Spur should explain the following observations: (1) The continuity of the stratigraphy from the deep basin up into the high, (2) the difference in sedimentation pattern between the margin and the high, and (3) the abrupt change from earlier sediment draping of the high, to later onlap of the flanks and no deposition on top. Late uplift of the high can explain these observations, while it is not clear how a contourite model can be applied. Thus, we believe that a Late Miocene/Pliocene dating for the formation of the bathymetric relief is reasonable.

4.6. Plate Strength of the Vøring Spur

Vertical movement around the high is recorded by disturbance of the sedimentation pattern, which occurs up to 350 km from the EJMFZ [*Breivik et al.*, 2008], (Figures 2 and 16). The high is shallowest next to the fracture zone, tapering down to the abyssal plain to the northeast (Figure 2). Uplift at one side in an oceanic transform zone can occur, e.g., at the Vema Fracture Zone [*Bonatti et al.*, 2005]. *Gernigon et al.* [2009] tested what the geometry would mean in terms of flexural plate bending with a free edge at the fracture zone and found an equivalent elastic plate thickness of 10–13 km. They argued that compression in the then active

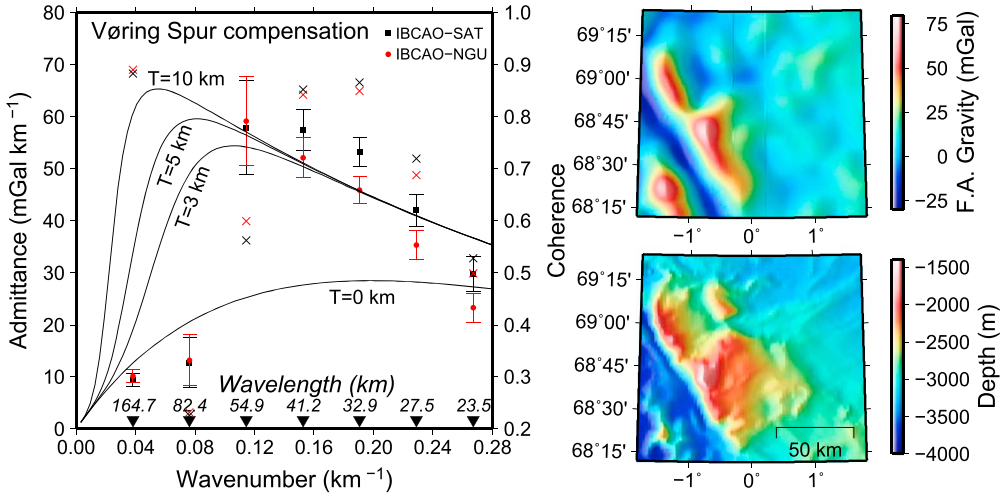

Figure 18. The admittance function (red and black filled symbols with 1σ error bars) between two different free-air gravity grids and IBCAO (v.2) bathymetry for the Vøring Spur. See text for details. On the right-hand side, we show the IBCAO (v.2) bathymetry and the DTU10 satellite gravity used. The results are compared to four different elastic plate thicknesses (0, 3, 5, and 10 km), documenting a very low plate strength. The coherence at the specific wavelengths is shown by crosses.

transform must have caused some of the observed vertical movement. That model would limit uplift to occur early: Late Eocene to Oligocene.

We estimate the plate strength with the program gravfft, using the 3-D admittance function between the bathymetry and free-air gravity [*Luis and Neves*, 2006]. The bathymetry grid is from IBCAO-2 ship track compilation [*Jakobsson et al.*, 2008], while gravity is either the DTU10 satellite-based grid [*Andersen et al.*, 2010; *Andersen*, 2010], or satellite data combined with ship track from the Norwegian Geological Survey (NGU) [*Skilbrei et al.*, 2000]. The results between the two combinations are comparable (Figure 18). There is low coherence at intermediate wavelengths, which may be due to the sediment burial of the basement core of the high. Still, the longest wavelength has high coherence, showing that the bathymetry is near local isostatic equilibrium.

Gernigon et al. [2009] also find low present plate strength but argue that the plate strength could have been greater in the past. However, if the present geometry is to be explained by flexural bending in the past, no weakening can occur, otherwise the plate deformation would relax. Thus, it appears that fracture zone compression cannot explain the present geometry. The elastic thickness of oceanic plates correlates with the temperature structure and increases with age [e.g., *Watts*, 1978]. If there was a magmatic event 20–30 Ma after the oceanic crust was created, intrusions would meet a plate with some strength, but the first inversion event would be of a young and weak plate. It is possible that because of this first event, and that the plate was still fairly young and hot under the second, the renewed magmatism was sufficient to keep the apparent plate strength low as observed.

4.7. Lack of Evidence for Early Eocene Triple Junction

In order to explain the formation of the Vøring Spur, *Gernigon et al.* [2009] invoked a triple junction with a leaky transform tied to the Mohn Ridge. The model was first proposed by *Olesen et al.* [2007], based on an apparent correlation between magnetic anomalies off the Vøring Plateau and off Traill Ø on the Northeast Greenland Margin. On the Norwegian side, the magnetic anomalies are tied to the seaward dipping reflector sequences, formed by flood basalts during the earliest seafloor spreading [e.g., *Talwani et al.*, 1983; *Planke and Eldholm*, 1994; *Berndt et al.*, 2001]. The offshore Northeast Greenland anomaly has not been studied, but the magnetic anomaly continues onshore onto the Traill Ø. Here the anomaly is tied to syenite intrusions that have been dated to ~35 Ma [*Noble et al.*, 1988; *Price et al.*, 1997], believed to relate to the rifting of the Jan Mayen microcontinent from Greenland. The magnetic anomalies on each side appear to be created by different processes at different times. Thus, the spatial correlation from East Greenland to the Vøring Plateau is coincidental, and the evidence for an Early Eocene triple junction is therefore lacking.

Gernigon et al. [2009] proposed that the Vøring Spur was formed later at the triple junction. Their model is presented as an extension of the early triple junction model of *Olesen et al.* [2007], but L. Gernigon (personal communication, 2012) pointed out that it does not depend on the early model being correct. A plate reconstruction model indicates that a triple junction could exist at a later stage [*Gaina et al.*, 2009], though the uncertainty seems too high to constrain a third plate boundary.

Gernigon et al. [2009] used the Azores triple junction as an analog for the Vøring Spur. Much of the anomalous magmatism occurs along the Terceira Rift, but there is also considerable Quaternary magmatism southeast of it [e.g., *Vogt and Jung*, 2004]. The Terceira Rift was established through rifting of older oceanic crust about 1 Ma ago, and extension rate is at ~4 mm a^{-1} ultraslow [*Vogt and Jung*, 2004]. The Azores Plateau has several elongated ridges subparallel to the Terceira Rift, up to several hundred kilometers long, and 20 to 40 km wide [*Lourenço et al.*, 1998]. The present rift location is at the northern edge of the magmatically active area, where the other ridges most likely are the result of rift jumps necessary to maintain the position over the Azores hot spot due to the southwestward absolute plate motion [*Vogt and Jung*, 2004; *Yang et al.*, 2006]. *Adam et al.* [2013] showed that the lithospheric stress field produced by the Azores plume convection pattern derived from mantle tomography [*Yang et al.*, 2006] is consistent with the location of the Terceira Rift. Thus, the mantle plume appears to both determine the rift location and to cause excess magmatism.

If the crustal thickness of the Vøring Spur dates back to the seafloor formation and taps the plume-driven anomalous breakup magmatism as *Gernigon et al.* [2009] proposed, it would result in a positive H-V_p correlation. As pointed out above, the velocity signature of the Vøring Spur is quite different from that of the breakup magmatism, showing that it was created by a different process. Thus, we find that the triple junction model is not confirmed by testing reasonable predictions drawn from it. Combined with our documentation that the timing of formation also has to be much younger, we have to conclude that the triple junction model is not applicable here.

5. Summary and Conclusions

In the year 2003, an OBS/H survey was acquired across the Vøring and Lofoten margins. Profile 11-03 presented here was shot across the outer Vøring Plateau and over the adjacent Vøring Spur in the oceanic basin. Results from *P* wave traveltime modeling of the data along the profile indicate a narrow transition from typical continental velocity to a higher oceanic velocity under the seaward dipping reflectors at the margin. The maximum oceanic crustal thickness is ~17 km next to the continent.

The lower crustal *P* wave velocity of the Vøring Spur is typical for gabbroic rocks, and the crust is up to 15 km thick. It could have been interpreted as simply a thickened oceanic crust, if it was not for the sedimentation pattern over and around it. The earliest sedimentary section is thick and drapes the high with stratigraphy more or less parallel to the basement. The later sequence onlaps the high but does not reach the top. This radical change in sedimentation shows that the present topography was created by later uplift. An episode of tentative Late Miocene/Pliocene magmatic underplating/intrusion apparently caused the inversion, also affecting a larger area NE of the Vøring Spur. The seismic data also reveal an earlier, lesser inversion event localized to the main high.

We correlate seismic velocity (V_p) and crustal thickness (H) in order to estimate the mantle melting degree. The thick oceanic crust at the Vøring Plateau margin shows a piecewise positive H-V_p correlation for profiles 10-03 [*Breivik et al.*, 2009] and 11-03. The older Profile 1-99 over the central Vøring Plateau shows a strong, positive H-V_p correlation, with an abrupt increase in V_p at the outer margin. All three profiles were also analyzed for V_p as a function of time. Results indicate that excess mantle melting was caused by elevated mantle temperature. However, the first 2 Ma after breakup show lower V_p than expected from the thickness, indicating that a secondary process enhanced the excess temperature-driven melting, possibly small-scale convection. At ~51–51.5 Ma, this process apparently ceased, and the remaining magmatic development may be explained solely by a finite mantle reservoir with elevated temperature being consumed by the seafloor spreading.

The H-V_p analysis of the Vøring Spur results in velocities that have little variation with crustal thickness, showing that the formation was not related to the temperature-dominated breakup magmatism. That precludes the triple junction model for the formation of the Vøring Spur proposed by *Gernigon et al.* [2009]. The

high is close to local isostatic equilibrium, showing that compression and flexural bending at the EJMFZ did not contribute significantly to the observed vertical movement. Formation of the Vøring Spur appears to be caused by late secondary magmatic growth derived from a moderate mantle melt degree, though the mechanism behind this event is uncertain.

Acknowledgments

We thank H. Shimamura, O. Ritzmann, and A. Krabbenhöft for their invaluable participation in planning, executing, and initial processing of the OBS data, and C. Zelt for the forward/inversion seismic modeling software. Thanks also goes to J.F. Luis for his gravfft program, to Laurent Gernigon at NGU for the JAS-05 magnetic survey, to the Norwegian Petroleum Directorate (NPD) for the side scan bathymetry and the LOS MCS lines, and to Robert White for the iSIMM Faeroes model. Finally, we would like to thank Editors Tom Parsons and Robert Nowack for handling the manuscript, as well as John Armitage, an anonymous reviewer, and the Associate Editor for their thorough reviews that helped to improve the manuscript. The OBS data can be obtained by contacting authors A.J. Breivik or R. Mjelde. The Research Council of Norway funded the wide-angle seismic survey under the European Science Foundation Euromargins program (CRP01). Additional funding was provided by the Large Scale Facility at GEOMAR, project HPRI-CT-2001-00154.

References

Adam, C., P. Madureira, J. M. Miranda, N. Lourenço, M. Yoshida, and D. Fitzenz (2013), Mantle dynamics and characteristics of the Azores plateau, *Earth Planet. Sci. Lett.*, *362*, 258–271, doi:10.1016/j.epsl.2012.11.014.

Andersen, O. B. (2010), The DTU10 gravity field and mean sea surface, paper presented at 2nd International Symposium of the Gravity Field of the Earth (IGFS2), Fairbanks, Alaska.

Andersen, O. B., P. Knudsen, and P. Berry (2010), The DNSC08GRA global marine gravity field from double retracked satellite altimetry models, *J. Geod.*, *84*(3), 191–199, doi:10.1007/s00190-009-0355-9.

Armitage, J. J., J. S. Collier, and T. A. Minshull (2010), The importance of rift history for volcanic margin formation, *Nature*, *465*, 913–917, doi:10.1038/nature09063.

Berndt, C., S. Planke, E. Alvestad, F. Tsikalas, and T. Rasmussen (2001), Seismic volcanostratigraphy of the Norwegian margin: Constraints on tectonomagmatic break-up processes, *J. Geol. Soc.*, *158*, 413–426.

Bonatti, E., D. Brunelli, W. R. Buck, A. Cipriani, P. Fabretti, V. Ferrante, L. Gasperini, and M. Ligi (2005), Flexural uplift of a lithospheric slab near the Vema transform (Central Atlantic): Timing and mechanisms, *Earth Planet. Sci. Lett.*, *240*, 642–655, doi:10.1016/j.epsl.2005.10.010.

Boutillier, R. R., and C. E. Keen (1999), Small-scale convection and divergent plate boundaries, *J. Geophys. Res.*, *104*(B4), 7389–7403.

Breivik, A. J., R. Mjelde, J. I. Faleide, and Y. Murai (2006), Rates of continental breakup magmatism and seafloor spreading in the Norway Basin—Iceland plume interaction, *J. Geophys. Res.*, *111*, B07102, doi:10.1029/2005JB004004.

Breivik, A. J., J. I. Faleide, and R. Mjelde (2008), Neogene magmatism northeast of the Aegir and Kolbeinsey Ridges, NE Atlantic: Spreading ridge—Mantle plume interaction?, *Geochem. Geophys. Geosyst.*, *9*, Q02004, doi:10.1029/2007GC001750.

Breivik, A. J., J. I. Faleide, R. Mjelde, and R. Flueh (2009), Magma productivity and early seafloor spreading rate correlation on the northern Vøring margin, Norway—Constraints on mantle melting, *Tectonophysics*, *468*, 206–223, doi:10.1016/j.tecto.2008.09.020.

Breivik, A. J., R. Mjelde, J. I. Faleide, and Y. Murai (2012), The eastern Jan Mayen microcontinent volcanic margin, *Geophys. J. Int.*, *188*, 798–818, doi:10.1111/j.1365-246X.2011.05307.x.

Brekke, H. (2000), The tectonic evolution of the Norwegian Sea continental margin with emphasis on the Vøring and Møre Basins, in *Dynamics of the Norwegian Margin*, vol. 167, edited by A. Nøttvedt et al., pp. 327–378, Geol. Soc. Spec. Publ. London, U. K.

Bruvoll, V., A. J. Breivik, R. Mjelde, and R. B. Pedersen (2009), Burial of the Mohn–Knipovich seafloor spreading ridge by the Bear Island fan: Time constraints on tectonic evolution from seismic stratigraphy, *Tectonics*, *28*, TC4001, doi:10.1029/2008TC002396.

Cande, S. C., and D. V. Kent (1995), Revised calibration of the geomagnetic polarity time scale for Late Cretaceous and Cenozoic, *J. Geophys. Res.*, *100*(B4), 6093–6095.

Christensen, N. I., and W. D. Mooney (1995), Seismic velocity structure and composition of continental crust: A global view, *J. Geophys. Res.*, *100*(B7), 9761–9788.

Eldholm, O., and K. Grue (1994), North Atlantic volcanic margins: Dimensions and production rates, *J. Geophys. Res.*, *99*(B2), 2955–2968.

Escartin, J., D. K. Smith, J. Cann, H. Schouten, C. H. Langmuir, and S. Escrig (2008), Central role of detachment faults in accretion of slow-spreading oceanic lithosphere, *Nature*, *455*, 790–294, doi:10.1038/nature07333.

Faugères, J.-C., D. A. V. Stow, P. Imbert, and A. Viana (1999), Seismic features diagnostic of contourite drifts, *Mar. Geol.*, *162*, 1–38.

Forsyth, D. A., P. Morel-A-L'Huissier, I. Asudeh, and A. G. Green (1986), Alpha ridge and Iceland—Products of the same plume?, *J. Geodyn.*, *6*, 197–214.

Fountain, D. M., and N. I. Christensen (1989), Composition of the continental crust and upper mantle: A Review, in *Geophysical Framework of the Continental United States*, vol. 172, edited by L. C. Pakiser and W. D. Mooney, pp. 711–742, Geol. Soc. Am., Boulder, Colo.

Gaina, C., L. Gernigon, and P. Ball (2009), Palaeocene—Recent plate boundaries in the NE Atlantic and the formation of the Jan Mayen microcontinent, *J. Geol. Soc.*, *166*, 601–616, doi:10.1144/0016-76492008-112.

Gernigon, L., O. Olesen, J. Ebbing, S. Wienecke, C. Gaina, J. O. Mogaard, M. Sand, and R. Myklebust (2009), Geophysical insights and early spreading history in the vicinity of the Jan Mayen fracture zone, Norwegian–Greenland Sea, *Tectonophysics*, *468*, 185–205, doi:10.1016/j.tecto.2008.04.025.

Haase, K. M., and C. W. Devey (1994), The petrology and geochemistry of Vesteris Seamount, Greenland Basin—An intraplate alkaline volcano of non-plume origin, *J. Petrol.*, *35*(2), 295–328.

Hinz, K., O. Eldholm, M. Block, and J. Skogseid (1993), Evolution of North Atlantic volcanic continental margins, in *Petroleum Geology of Northwest Europe, Proceedings of the 4th Conference*, edited by J. R. Parker, pp. 901–913, Geol. Soc. London, U. K.

Hirschmann, M. M. (2010), Partial melt in the oceanic low velocity zone, *Phys. Earth Planet. Inter.*, *179*, 60–71, doi:10.1016/j.pepi.2009.12.003.

Hjelstuen, B. O., O. Eldholm, and J. I. Faleide (2007), Recurrent Pleistocene mega-failures on the SW Barents sea margin, *Earth Planet. Sci. Lett.*, *258*, 605–618, doi:10.1016/j.epsl2007.04.025.

Holbrook, W. S., et al. (2001), Mantle thermal structure and active upwelling during continental breakup in the North Atlantic, *Earth Planet. Sci. Lett.*, *190*, 251–266.

Hooft, E. E. E., R. S. Detrick, D. R. Toomey, J. A. Collins, and J. Lin (2000), Crustal thickness and structure along three contrasting spreading segments of the mid-Atlantic ridge, 33.5°–35°N, *J. Geophys. Res.*, *105*(B4), 8205–8226.

Jacobson, R. S. (1992), Impact of crustal evolution on changes of the seismic properties of the uppermost oceanic crust, *Rev. Geophys.*, *30*(1), 23–42.

Jakobsson, M., R. Macnab, L. Mayer, R. Anderson, M. Edwards, J. Hatzky, H. W. Schenke, and P. Johnson (2008), An improved bathymetric portrayal of the Arctic Ocean: Implications for ocean modeling and geological, geophysical and oceanographic analyses, *Geophys. Res. Lett.*, *35*, L07602, doi:10.1029/2008GL033520.

Kelemen, P. B., and W. S. Holbrook (1995), Origin of thick, high-velocity, igneous crust along the U.S. East Coast Margin, *J. Geophys. Res.*, *100*(B7), 10,077–10,094.

Key, K., S. Constable, L. Liu, and A. Pommier (2013), Electrical image of passive mantle upwelling beneath the northern East Pacific rise, *Nature*, *495*, 499–502, doi:10.1038/nature11932.

Klein, E. M., and C. H. Langmuir (1987), Global correlations of ocean ridge basalt chemistry with axial depth and crustal thickness, *J. Geophys. Res.*, *92*(B8), 8089–8115.
Kodaira, S., R. Mjelde, K. Gunnarsson, H. Shiobara, and H. Shimamura (1998), Structure of the Jan Mayen microcontinent and implication for its evolution, *Geophys. J. Int.*, *132*, 383–400.
Kohlstedt, D. L., and B. K. Holtzman (2009), Shearing melt out of the Earth: An experimentalist's perspective on the influence of deformation on melt extraction, *Annu. Rev. Earth Planet. Sci.*, *37*, 561–593, doi:10.1146/annurev.earth.031208.100104.
Korenaga, J., P. B. Kelemen, and W. S. Holbrook (2002), Methods for resolving the origin of large igneous provinces from crustal seismology, *J. Geophys. Res.*, *107*(B9), 2178, doi:10.1029/2001JB001030.
Laberg, J. S., T. Dahlgren, T. O. Vorren, H. Haflidason, and P. Bryn (2001), Seismic analyses of Cenozoic contourite drift development in the northern Norwegian Sea, *Mar. Geophys. Res.*, *22*, 401–416.
Laberg, J. S., et al. (2005), Cenozoic alongslope processes and sedimentation on the NW European Atlantic margin, *Mar. Pet. Geol.*, *22*, 1069–1088.
Lawver, L. A., and R. D. Müller (1994), Iceland hotspot track, *Geology*, *22*, 311–314.
Lourenço, N., J. M. Miranda, J. F. Luis, A. Ribeiro, L. A. Mendes Victor, J. Madeira, and H. D. Needham (1998), Morpho-tectonic analysis of the Azores Volcanic Plateau from a new bathymetric compilation of the area, *Mar. Geophys. Res.*, *20*, 141–156.
Ludwig, W. I., J. E. Nafe, and C. L. Drake (1970), Seismic refraction, *Sea*, *4*(1), 53–84.
Luis, J. F., and M. C. Neves (2006), The isostatic compensation of the Azores Plateau: A 3D admittance and coherence analysis, *J. Volcanol. Geotherm. Res.*, *156*, 10–22.
McKenzie, D., and M. J. Bickle (1988), The volume and composition of melt generated by extension of the lithosphere, *J. Petrol.*, *29*(3), 625–679.
Mertz, D. F., W. D. Sharp, and K. M. Haase (2004), Volcanism on the Eggvin Bank (Central Norwegian-Greenland Sea, latitude ~71°N): Age, source, and relationship to the Iceland and putative Jan Mayen plumes, *J. Geodyn.*, *38*, 57–83, doi:10.1016/j.jog.2004.03.003.
Mjelde, R., P. Digranes, M. van Schaack, H. Shimamura, S. Shiobara, H. Kodaira, O. Naess, N. Sørenes, and E. Vågnes (2001), Crustal structure of the outer Vøring Plateau, offshore Norway, from ocean bottom seismic and gravity data, *J. Geophys. Res.*, *106*(B4), 6769–6791.
Mjelde, R., T. Raum, B. Myhren, H. Shimamura, Y. Murai, T. Takanami, R. Karpuz, and U. Næss (2005), Continent-ocean transition on the Vøring Plateau, NE Atlantic, derived from densely sampled ocean bottom seismometer data, *J. Geophys. Res.*, *110*, B05101, doi:10.1029/2004JB003026.
Mosar, J., E. A. Eide, P. T. Osmundsen, A. Sommaruga, and T. H. Torsvik (2002), Greenland Norway separation: A geodynamic model for the North Atlantic, *Norw. J. Geol.*, *82*, 282–299.
Mutter, J. C., and C. M. Zehnder (1988), Deep crustal structure and magmatic processes: The inception of seafloor spreading in the Norwegian–Greenland Sea, in *Early Tertiary Volcanism and Opening of the NE Atlantic, Geol. Soc. London Spec. Publ.*, vol. 39, edited by A. C. Morton and L. M. Parsons, pp. 35–48, London, U. K.
Mutter, J. C., W. R. Buck, and C. M. Zehnder (1988), Convective partial melting: 1. A model for the formation of thick basaltic sequences during the initiation of spreading, *J. Geophys. Res.*, *93*(B2), 1031–1048.
Naif, S., K. Key, S. Constable, and R. L. Evans (2013), Melt-rich channel observed at the lithosphere-asthenosphere boundary, *Nature*, *495*, 356–359, doi:10.1038/nature11939.
Noble, R. H., R. M. Macintyre, and P. E. Brown (1988), Age constraints on Atlantic evolution: Timing of magmatic activity along the E Greenland continental margin, *Geol. Soc. Spec. Publ.*, *39*, 201–214, doi:10.1144/GSL.SP.1988.039.01.19.
Olesen, O., J. Ebbing, E. Lundin, E. Mauring, J. R. Skilbrei, T. H. Torsvik, E. K. Hansen, T. Henningsen, P. Midbøe, and M. Sand (2007), An improved tectonic model for the Eocene opening of the Norwegian-Greenland sea: Use of modern magnetic data, *Mar. Pet. Geol.*, *24*, 53–66, doi:10.1016/j.marpetgeo.2006.10.008.
Parkin, C. J., and R. S. White (2008), Influence of the Iceland mantle plume on oceanic crust generation in the north Atlantic, *Geophys. J. Int.*, *173*, 168–188, doi:10.1111/j.1365-246X.2007.03689.x.
Parkin, C. J., Z. C. Lunnon, R. S. White, P. A. F. Christie, and iSIMM Team (2007), Imaging the pulsing Iceland mantle plume through the Eocene, *Geology*, *35*(1), 93–96, doi:10.1130/G23273A.1.
Planke, S., and O. Eldholm (1994), Seismic response and construction of seaward dipping wedges of flood basalts: Vøring volcanic margin, *J. Geophys. Res.*, *99*, 9263–9278.
Price, S., J. Brodie, A. Whitham, and R. Kent (1997), Mid-Tertiary rifting and magmatism in the Traill Ø region, East Greenland, *J. Geol. Soc.*, *154*, 419–434.
Roberts, A. W., R. S. White, and P. A. F. Christie (2009), Imaging igneous rocks on the north Atlantic rifted continental margin, *Geophys. J. Int.*, *179*, 1024–1038, doi:10.1111/j.1365-246X.2009.04306.x.
Sallarès, V., P. Charvis, E. R. Flueh, and J. Bialas (2003), Seismic structure of Cocos and Malpelo Volcanic Ridges and implications for hot spot-ridge interaction, *J. Geophys. Res.*, *108*(B12), 2564, doi:10.1029/2003JB002431.
Sallarès, V., P. Charvis, E. R. Flueh, J. Bialas, and the SALIERI Scientific Party (2005), Seismic structure of the Carnegie Ridge and the nature of the Galápagos hotspot, *Geophys. J. Int.*, *161*, 763–788, doi:10.1111/j.1365-246X.2005.02592.x.
Sandwell, D. T., and W. H. F. Smith (1997), Marine gravity anomaly from Geosat and ERS 1 satellite altimetry, *J. Geophys. Res.*, *102*(B5), 10,039–10,054.
Schmerr, N. (2012), The Gutenberg discontinuity: Melt at the lithosphere-asthenosphere boundary, *Nature*, *335*, 1480–1483, doi:10.1126/science.1215433.
Skilbrei, J. R., O. Kihle, O. Olesen, J. Gellein, A. Sindre, D. Solheim, and B. Nyland (2000), *Gravity Anomaly Map, Norway and Adjacent Areas, Scale 1:3 Million*, Geol. Surv. Norway, Trondheim, Norway.
Skogseid, J. (1994), Dimensions of the Late Cretaceous–Palaeocene northeast Atlantic rift derived from Cenozoic subsidence, *Tectonophysics*, *240*, 225–247.
Smallwood, J. R., and R. S. White (2002), Ridge-Plume interaction in the North Atlantic and its influence on continental breakup and seafloor spreading, in *The North Atlantic Igneous Province: Stratigraphy, Tectonic, Volcanic and Magmatic Processes, Geol. Soc. London Spec. Publ.*, vol. 197, edited by D. W. Jolley and B. R. Bell, pp. 15–37, London, U. K.
Smith, W. H. F., and P. Wessel (1990), Gridding with continuous curvature splines in tension, *Geophysics*, *55*(3), 293–305.
Stixrude, L., and C. Lithgow-Bertelloni (2005), Mineralogy and elasticity of the oceanic upper mantle: Origin of the low-velocity zone, *J. Geophys. Res.*, *110*, B03204, doi:10.1029/2004JB002965.
Storey, M., R. A. Duncan, and C. Tegner (2007), Timing and duration of volcanism in the North Atlantic Igneous Province: Implications for geodynamics and links to the Iceland hotspot, *Chem. Geol.*, *241*, 264–281, doi:10.1016/j.chemgeo.2007.01.016.

Stow, D. A. V., J.-C. Faugères, E. Gonthier, M. Cremer, E. Llave, F. J. Hernández-Molina, L. Somoza, and V. Díaz-Del-Río (2002), Faro-Albufeira Drift Complex, Northern Gulf of Cadiz, in *Deep-Water Contourite Systems: Modern Drifts and Ancient Series, Seismic and Sedimentary Characteristics, Geol. Soc. London Mem. 22*, edited by D. A. V. Stow et al., pp. 137–154, Geol. Soc. London, London, U. K.

Talwani, M., K. Hinz, and J. Mutter (1983), Ocean continent boundary under the Norwegian continental margin, in *Structure and Development of the Greenland–Scotland Ridge: New Methods and Concepts*, edited by M. H. P. Bott, S. Saxov, and M. Talwani, pp. 121–131, Plenum Press, New York.

Trønnes, R. G., S. Planke, B. Sundvoll, and P. Imsland (1999), Recent volcanic rocks from Jan Mayen: Low-degree melt fractions of enriched northeast Atlantic mantle, *J. Geophys. Res.*, *104*(B4), 7153–7168.

Verhoef, J., W. R. Roest, R. Macnab, J. Arkani-Hamed, and Project Team (1996), Magnetic anomalies of the Arctic and North Atlantic Oceans and adjacent land areas, *Tech. Rep.*, Geol. Surv. Canada, Dartmouth, NS, Canada.

Vogt, P. R., and W. Y. Jung (2004), The Terceira Rift as hyper-slow, hotspot-dominated oblique spreading axis: A comparison with other slow-spreading plate boundaries, *Earth Planet. Sci. Lett.*, *218*, 77–90, doi:10.1016/S0012-821X(03)00627-7.

Voss, M., and W. Jokat (2007), Continent-ocean transition and voluminous magmatic underplating derived from P-wave velocity of the East Greenland continental margin, *Geophys. J. Int.*, *170*, 580–604, doi:10.1111/j.1365-246X.2007.03438.x.

Watts, A. B. (1978), An analysis of isostasy in the world's oceans 1. Hawaiian—Emperor seamount chain, *J. Geophys. Res.*, *83*(B12), 5989–6004.

Wessel, P., and W. H. F. Smith (1998), New, improved version of Generic Mapping Tools released, *Eos Trans. AGU*, *79*, 579.

White, R., D. Spence, S. R. Fowler, D. McKenzie, G. K. Westbrook, and A. Bowen (1987), Magmatism at rifted continental margins, *Nature*, *330*, 439–444.

White, R. S. (1989), Initiation of the Iceland plume and opening of the North Atlantic, in *Extensional Tectonics and Stratigraphy of the North Atlantic Margins*, edited by A. J. Tankard and H. R. Balkwill, pp. 149–154, AAPG Mem., No. 46, Tulsa, Okla.

White, R. S., L. K. Smith, A. W. Roberts, P. A. F. Christie, N. J. Kusznir, and iSIMM Team (2008), Lower-crustal intrusion on the North Atlantic continental margin, *Nature*, *452*, 460–464, doi:10.1038/nature06687.

Wilkens, R. H., G. J. Fryer, and J. Karsten (1991), Evolution of porosity and seismic structure of upper oceanic crust: Importance of aspect ratios, *J. Geophys. Res.*, *96*(B11), 17,981–17,995.

Yang, T., Y. Shen, S. van der Lee, S. C. Solomon, and S.-H. Hung (2006), Upper mantle structure beneath the Azores hotspot from finite-frequency seismic tomography, *Earth Planet. Sci. Lett.*, *250*, 11–26, doi:10.1016/j.epsl.2006.07.031.

Zehnder, C. M., J. C. Mutter, and P. Buhl (1990), Deep seismic and geochemical constraints on the nature of rift-induced magmatism during breakup of the North Atlantic, *Tectonophysics*, *173*, 545–565.

Zelt, C. A., and R. B. Smith (1992), Seismic traveltime inversion for 2-D crustal velocity structure, *Geophys. J. Int.*, *108*, 16–34.